Available online at www.sciencedirect.com
ScienceDirect
Geochimica et Cosmochimica Acta 70 (2006) 5437–5454
Geochimica
www.elsevier.com/locate/gca

Transport of radionuclides in an unconfined chalk aquifer inferred from U-series disequilibria

Amélie Hubert [a,b,*], Bernard Bourdon [b,1], Eric Pili [a], Laure Meynadier [b]

[a] *Département Analyse Surveillance Environnement, Commissariat à l'Energie Atomique, BP 12, 91680 Bruyères-le-Châtel, France*
[b] *Laboratoire de Géochimie et Cosmochimie (UMR 7579 CNRS), Institut de Physique du Globe de Paris, Université Paris 7 Denis Diderot, 4 place Jussieu, 75252 Paris Cedex 05, France*

Received 28 June 2005; accepted in revised form 7 August 2006

Abstract

U-series disequilibria measured in waters and rocks from a chalk aquifer in France have been used as an analog for long-term radionuclide migration. Drill core samples from a range of depths in the vadose zone and in the saturated zone, as well as groundwater samples were analyzed for ^{238}U, ^{234}U, ^{232}Th and ^{230}Th to determine transport mechanisms at the water/rock interface and to quantify parameters controlling the migration of radionuclides. Isotope measurements in rocks were done by TIMS, whereas ($^{234}U/^{238}U$) and ($^{230}Th/^{232}Th$) activity ratios in water samples were measured by multi-collector-ICP-MS. Both depletion and enrichment in ^{234}U relative to ^{238}U were observed in carbonate rock samples resulting from chemical weathering in the unsaturated zone and calcite precipitation in the zone of water-table oscillation, respectively. The correlation between ($^{230}Th/^{232}Th$) activity ratios and $^{87}Sr/^{86}Sr$ ratios found in the chalk samples indicates that thorium is mainly contained in a minor silicate phase whose abundance is variable in chalk samples. Water samples are all characterized by ($^{234}U/^{238}U$) > 1 resulting from α-recoil effect of ^{234}Th. Groundwaters are characterized by a more radiogenic signature in $^{87}Sr/^{86}Sr$ than the rocks. Moreover, ($^{230}Th/^{232}Th$) activity ratios in the waters are lower than in the rocks, and increase with distance from the water divide, which suggests that Th transport is controlled by colloids formed during water infiltration in the soil. A 1-D transport model has been developed in order to constrain the U-series nuclide transport considering a transient behavior of radionuclides in the aquifer and a time-dependent composition for the solid phase. This model permits a prediction of the time scale of equilibration of the system, and an estimation of parameters such as weathering rate, distribution coefficients and α-recoil fractions. Retardation factors of 10–35 and from 1×10^4 to 2×10^5 were predicted for U and Th, respectively, and can be used to predict the migration of radionuclides released as contaminants in the environment. At the scale of our watershed (~32 km^2), a characteristic migration time from recharge to riverine discharge of 200–600 yr for U and 0.2–3.7 Myr for Th was obtained.

1. Introduction

The short-term fate of radionuclides in aquifers has been studied in considerable detail either through laboratory experiments or through numerical models calibrated and validated based on field data extending up to 50 years (e.g., Zielinski and Rosholt, 1978; Buddemeier, 1988; Kersting et al., 1999). In contrast, studies of long-term migration (>50 years) are scarce and usually rely on chemical analogs (e.g., Liu et al., 1996). U-series nuclides are especially powerful in investigating these issues as they represent natural analogs that have been migrating in aquifer systems over long time scales (e.g., Krishnaswami et al., 1982; Ku et al., 1992). Thus, they should enable investigation of the processes involved in long-term radionuclide transport over large spatial scales. The U-series decay chains include elements with a wide range of chemical properties as well as isotopes with differing half-lives. Among them, we have studied the longer-lived isotopes of uranium (U) and thorium (Th). In a closed system, all the nuclides in the decay chain reach secular equilibrium,

* Corresponding author.
E-mail address: amelie.hubert@cea.fr (A. Hubert).
[1] Present address: Institute of Isotope Geochemistry and Mineral Resources, ETH Zurich, 8092 Zurich, Switzerland.

0016-7037/$ - see front matter © 2006 Elsevier Inc. All rights reserved.
doi:10.1016/j.gca.2006.08.008

i.e., the activities of the radionuclides are equal. As water flows through an aquifer, disequilibria (i.e., fractionation) between U-series nuclides are produced by chemical and physical processes such as weathering, adsorption, desorption or α-recoil. This allows the assessment of both the temporal and spatial scales of these processes (Ku et al., 1992; Osmond and Cowart, 1992; Osmond and Ivanovich, 1992; Bourdon et al., 2003; Porcelli and Swarzenski, 2003).

U-series disequilibria have been used in several studies of radionuclide behavior in groundwater (Krishnaswami et al., 1982; Copenhaver et al., 1993; Luo et al., 2000). These studies describe the transport processes (adsorption, desorption, α-recoil, dissolution, and precipitation) that produce U-series disequilibria measured in water and use a mass-balance approach to estimate some of these parameters, where the α-recoil inputs are derived from ^{222}Rn measurements. More recently, Tricca et al. (2000) developed a transport model including an advective term to the processes of retardation described above. This model has been applied to the studies of sandy aquifers (Tricca et al., 2001; Reynolds et al., 2003) by considering that the system is at steady state in order to solve the transport equations.

Previous studies were based on measurements of U- and Th-series nuclides in groundwaters and assumption of a solid phase with uniform U, Th concentrations and at secular equilibrium. In contrast to these previous studies, we, in addition to water sampling, have done a comprehensive sampling of the solid phase from boreholes within a chalk aquifer in the Paris Basin (France), and analyzed them for U and Th isotopes. The sampling of both the solid and fluid phases of the aquifer should provide a better understanding of the behavior of radionuclides at the water/rock interface, which is the key for the development of a robust mass-balance model. Unlike the model of Tricca et al. (2000), which assumes steady state with a solid of constant chemical composition, our model allows transient behavior and includes a proper mass balance for both solid and fluid. This model was then used to evaluate key parameters influencing the transport of radionuclides in an unconfined calcareous aquifer.

2. Geological setting and sampling of the chalk aquifer

The Upper Cretaceous chalk aquifer extends over an area of 70,000 km^2 in the Paris Basin. The chalk aquifer has been extensively studied in England (Cuttell et al., 1986; Edmunds et al., 1987; Feast et al., 1997; Elliot et al., 1999; Schürch et al., 2004) but there are only a few isotopic studies on the continental part of this aquifer (Kloppmann et al., 1996, 1998). Chalk is characterized by having double porosity (matrix and fractures) providing pathways for both slow and rapid migration of water. The rock has its own matrix porosity (first type of porosity) and this rock is fractured, which is the second type of porosity. The total porosity of the chalk is about 40% (Crampon et al., 1993a), whereas the fracture porosity is about 1%. Price et al. (1993) indicate that 15% of the recharge to the chalk aquifer takes place through fractures. In the saturated zone, both matrix and fractures are filled with water. In the unsaturated zone, fractures are empty and matrix porosity is saturated due to high pressure in the capillary fringe that extends up to 40 m (Vachier et al., 1987). Above the capillary fringe, the matrix is only partly saturated.

The study area corresponds to a watershed located in the Champagne region (NE of France). In this region, the aquifer is monolithological (Campanian chalk, mostly calcium carbonate), which makes it ideally suited for studying water/rock interaction. This aquifer is unconfined and is an important groundwater resource in France (Crampon et al., 1993b). The studied watershed extends 8 km N–S and about 4 km E–W (Fig. 1a). The recharge area is located mainly on mounts forming the southern boundary of the catchment divide (Fig. 1a). Water flows in a SW–NE direction and the aquifer is bounded on the north by the Suippe river. The boreholes used for sampling are located at the southern end of the watershed, near the catchment divide, mainly in a north–south trending dry valley.

The water flow velocity has been determined based on the hydraulic conductivity and the effective porosity of the chalk. Pumping tests were done in the area and the chalk presents a hydraulic conductivity ranging between 1.5×10^{-6} and 1.5×10^{-5} m s^{-1}, with an effective porosity of 0.5–2% (Little et al., 1996). The effective flow velocity ranges between 30 and 1200 m yr^{-1}. Dry valleys are known to be major drains of the aquifer as the permeability is higher than in the surroundings (Crampon et al., 1993a). An average flow velocity of 450 m yr^{-1} was used in this work.

In order to analyze rocks at different depths, samples were taken from 80 mm diameter cores obtained from both new and older boreholes. Five bores, located along an approximate flow line (SSW to N, Figs. 1a and b), were drilled down to 45–80 m depth, depending on the topography and the piezometric level. Rock samples were taken from the center of these cores to avoid contamination by the drilling fluid (water from a nearby well). The chalk material has a mean grain radius of 0.38 μm and a density of 2700 kg m^{-3} (Vachier et al., 1979).

Water samples were collected only from newly drilled boreholes. These boreholes were carefully lined with PVC slotted lining from the base of the hole up to 10 m above the higher water level (measured on site) and with full lining up to 1 m above the topographic surface. The gap between the wall-rock and the PVC lining was filled with silica sand to prevent the hole from collapsing and to allow good water circulation from the base up to 1 m above the limit between slotted and full lining. Granules of bentonite were added in the last meter to avoid water infiltration from the surface. Cement was added to fill in the hole up to the top and stabilize the well. Upon completion, these wells were flushed using an air lift for over 1 h to clean them. After 5 months, the wells were pumped to purge

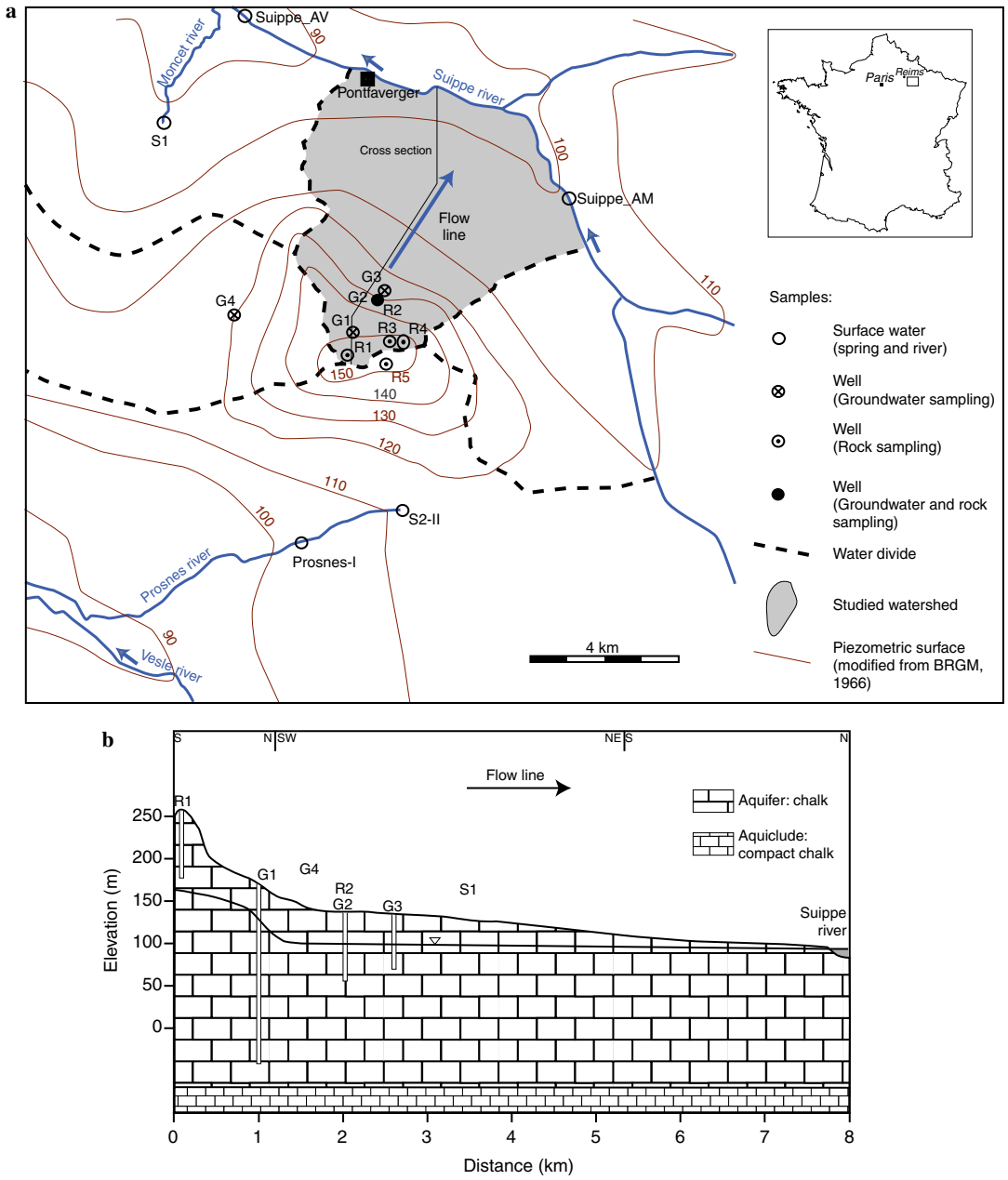

Fig. 1. (a) Map showing the studied area with the sampling locations. The piezometric level, shown in the figure, was determined during the dry season, and modified from BRGM (1966). (b) Cross-section along a flow line showing the water table and the piezometers used in this study.

them and minimize aging and adsorption of elements during water storage. Sampling was done 24–48 h after the purging, which allow the water level in the well to come back to its original level. Sampling was performed 10 m below the water table or 1 m above the bottom of the well when the water was low. During groundwater sampling, pH and conductivity were measured to ensure that constant conditions were reached. Just after sampling, pH, conductivity, temperature and redox potential were measured in situ, using a probe installed in the well at the depth of sampling.

Surface waters (springs S1, S2 and rivers Suippe, Prosnes and Vesle) as well as groundwaters (G1, G2, G3 and G4) were sampled in October 2002, October 2003 (periods of low water flow regime) and/or March 2003 (period of high water flow regime). The Prosnes sampling point (Fig. 1) was a river resurgence (Prosnes-I) in October and a spring (S2-II) in March. Twenty liters of water was sampled and then filtered with 0.45 μm filters by frontal filtration within 2 h of sampling in our field laboratory and stored in acid-washed polypropylene bottles. Two aliquots were acidified to pH $\leqslant$ 2 with high-purity HNO_3 for major cation and isotope measurements. Un-acidified aliquots were used for alkalinity determination by Gran titration in our field laboratory and for major anion analyses. For U and Th isotope analysis, they were preconcentrated from

Table 1
Chemical compositions of water samples

Sample name	Sampling date	Water type[a]	Alkalinity (mmol/L)	pH	Eh (mV)	Specific conductivity (mS cm^{-1})	Temperature (°C)	F^-	Cl^-	NO_3^-	SO_4^{2-}	Na^+	K^+	Mg^{2+}	Ca^{2+}	Balance (%)[b]	$\Omega_{calcite}$[c]
S1-I	9/23/02	S	4.45	7.09	517.3	0.438	11.4	36.6	495	414	165	188	42.0	46.8	2255	−8.4	−0.26
S1-II	3/18/03	S	3.55	7.21	461.6	0.557	10.2	19.1	481	548	154	207	39.7	48.7	2342	1.2	−0.22
Prosnes-I	10/8/02	R	3.87	7.13	491.6	0.064	9.3	43.3	639	463	123	198	37.4	35.1	2292	3.6	−0.27
S2-II	3/18/03	S	3.92	7.06	445.6	0.695	10.1	15.5	947	726	142	353	14.5	34.9	2816	1.5	−0.26
SuippeAM-I	9/23/02	R	3.89	8.04	555.8	0.424	11.9	14.4	587	422	100	230	32.0	33.0	2184	4.3	0.63
SuippeAM-II	3/18/03	R	4.48	7.78	483.5	0.574	8.3	13.3	607	557	113	236	34.7	37.6	2410	6.5	0.45
SuippeAV-I	9/23/02	R	3.57	7.74	557.5	0.445	12.0	19.5	605	432	122	280	55.5	43.2	2264	0.8	0.31
SuippeAV-II	3/18/03	R	3.56	7.83	526.1	0.579	9.1	13.4	608	542	115	247	39.2	42.6	2405	2.3	0.41
VesleAM-I	10/8/02	R	3.91	7.70	—	0.075	8.3	16.6	685	482	121	213	30.0	33.9	2302	−4.1	0.30
VesleAV-I	10/8/02	R	4.41	7.69	—	0.497	9.2	27.3	726	445	185	335	57.5	49.7	2626	−2	0.39
G1-II	3/20/03	GW	2.85	—	—	—	—	22.8	124	188	77	129	11.4	48.4	1693	4.1	−5.1[d]
G2-II	3/18/03	GW	3.68	7.02	480.4	0.538	11.3	14.1	181	328	34	170	10.9	57.6	2108	2.7	−0.43
G2-III	10/29/03	GW	3.8	7.42	499.1	0.414	11.4	5.3	237	290	19	165	10.3	49.4	2161	2.5	0.00
G3-III	10/30/03	GW	4.59	7.27	456.0	0.522	11.1	10.5	922	289	42	122	12.8	41.1	1664	−6.2	−0.18
G4-III	10/30/03	GW	3.54	7.50	517.3	0.400	11.0	26.3	302	576	48	174	74.4	49.4	2136	0.9	0.04

All concentrations are in μmol/L.

[a] S, spring; R, river; GW, groundwater.

[b] Cation/anion balance $= (\sum\text{cations} - \sum\text{anions})/(\sum\text{cations} + \sum\text{anions})$ in mEq L^{-1}.

[c] $\Omega_{calcite} = \log(a_{Ca^{2+}} \times a_{CO_3^{2-}}/K_S)$ with $a_{Ca^{2+}}$ and $a_{CO_3^{2-}}$ the activities of the ions and K_S the solubility constant of calcite.

[d] pH and temperature has been taken at 7.3 and 11.2, respectively (mean of groundwater values), for saturation index calculations.

10 to 15 L of filtered water with Fe hydroxide in our field laboratory; for this, 1 ml of a $Fe(NO_3)_3$ solution containing 40 mg/ml of high-purity Fe was added and distilled NH_4OH to adjust the pH to 9–9.5 for Fe hydroxide co-precipitation.

In order to characterize the composition of waters percolating from the surface, 20 g of soil material was mixed with about 0.1 L of rain water collected during the previous day. This mixture was then stirred and left for 2 h. The water was filtered with 0.45 μm filter and acidified to pH $\leqslant 2$ with high-purity HNO_3. Analytical procedures are described in Appendix A.

3. Results

Major element compositions of groundwater, river- and spring-water samples are given in Table 1. The cation/anion balance for the waters is better than 9% (Table 1), indicating a consistent data set. All the waters were oxidizing (Eh above 400 mV) and pH values range from 7 to 8. Water temperatures range between 8 and 12 °C, with no measurable variation between low and high flow regimes. The U, Th contents and the U-series activity ratios for water and rock samples are reported in Tables 2 and 3, respectively. The results of bulk rock analysis integrate both the carbonate and the residue after acetic acid dissolution (see Appendix A for details). In what follows, we refer to the bulk solid phase as chalk or rock samples. ($^{234}U/^{238}U$) ratios (where parentheses denote activity ratios) range from 0.878 to 1.109 in rock samples and from 0.981 to 1.541 in water samples. ($^{234}U/^{238}U$) ratios were measured along a depth profile (Fig. 2). In order to compare rock samples, the depth of the chalk was calculated relative to the mean water-table level for each well. Three zones can be identified in the aquifer: (i) a vadose zone, from 50 to 12 m above the mean water-table level, with chalk samples depleted in ^{234}U relative to ^{238}U, (ii) a saturated zone, from 9 m below the mean water-table down to the deepest sample (32 m), with chalk samples that have ($^{234}U/^{238}U$) above 1 or near secular equilibrium, and (iii) a zone of water-table fluctuation, between the upper part and the saturated zone, where chalk U activity ratios are both enriched and depleted in ^{234}U relative to ^{238}U. Water samples all show ($^{234}U/^{238}U$) > 1 (except for G1-II) with the highest values in river waters and the lowest value in the deepest groundwater sample. Such enrichments in ^{234}U in the dissolved phase have commonly been found in most groundwaters (Andrews and Kay, 1982; Plater et al., 1992; Bonotto and Andrews, 1993; Riotte and Chabaux, 1999). The soil leachate has a deficit in ^{234}U (as indicated above the aquifer in Fig. 2).

The chalk has a wide range in ($^{238}U/^{232}Th$) from 1.42 to 7.39 (Table 3), but ($^{230}Th/^{238}U$) ranging from just 1 to 2 (Fig. 3). A depth profile of ($^{230}Th/^{232}Th$) for both rock and water samples shows that water and rock samples do not have the same Th isotope signature (Fig. 4). Groundwaters have substantially lower ($^{230}Th/^{232}Th$) than the chalk, but similar ($^{230}Th/^{232}Th$) to the soil leachate and the fracture wall material. The only exception is a spring (S2-II) that was sampled 6.5 km from the water divide, quite far from the other sample locations.

4. Uranium/thorium behavior in the aquifer

In this section, we investigate qualitatively the geochemical behavior and fractionation pattern of U-series nuclides (^{238}U–^{234}U–^{230}Th) in the aquifer system. Variable ($^{234}U/^{238}U$) in the chalk indicate U mobility in the matrix over the past 1 Myr. Signatures of U mobility prior to 1 Myr cannot be detected as ^{234}U would have attained equilibrium with ^{238}U because of the short half-life of ^{234}U (≈245 kyr). Preferential leaching of ^{234}U in the vadose

Table 2
U-series and Sr isotope data in water samples

Sample name	Depth of sampling (m)	Distance from catchment divide (m)[b]	($^{234}U/^{238}U$)	($^{230}Th/^{232}Th$)	Th (pg L^{-1})	U (ng L^{-1})	$^{87}Sr/^{86}Sr$
S1-I[a]	0	3500	1.211 ± 0.002	3.87 ± 0.18	59.4 ± 0.9	466.2 ± 0.3	—
S1-II[a]	0	3500	1.209 ± 0.003	2.70 ± 0.17	90.5 ± 2.2	464.6 ± 0.4	—
SuippeAM-I	0	—	1.537 ± 0.003	2.82 ± 0.32	614.8 ± 12.2	259.4 ± 0.3	—
SuippeAM-II	0	—	1.472 ± 0.003	2.41 ± 0.03	84.7 ± 1.8	292.2 ± 0.2	0.707672 ± 21
SuippeAV-I	0	—	1.541 ± 0.003	2.87 ± 0.47	145.1 ± 2.0	304.2 ± 0.4	—
SuippeAV-II	0	—	1.498 ± 0.005	2.30 ± 0.14	11.8 ± 2.8	331.1 ± 0.4	0.707684 ± 17
Prosnes-I[a]	0	—	1.521 ± 0.003	2.66 ± 0.10	139.8 ± 8.4	434.8 ± 0.3	
S2-II[a]	0	6500	1.413 ± 0.002	11.00 ± 0.21	125.1 ± 2.8	308.5 ± 0.2	0.707658 ± 25
VesleAM-I[a]	0	—	1.461 ± 0.003	2.80 ± 0.17	177.7 ± 7.9	253.5 ± 0.2	—
VesleAV-I[a]	0	—	1.439 ± 0.003	3.20 ± 0.07	167.4 ± 10.0	390.5 ± 0.3	—
G1-II	70	1100	0.981 ± 0.002	3.05 ± 0.12	262.9 ± 3.8	823.8 ± 0.05	0.707556 ± 23
G2-II	45	2000	1.278 ± 0.002	1.85 ± 0.07	48.3 ± 12.2	932.0 ± 1.0	0.707821 ± 18
G2-III	50	2000	1.339 ± 0.002	2.73 ± 0.10	127.6 ± 2.6	643.3 ± 0.4	0.707815 ± 23
G3-III	46	2500	1.400 ± 0.004	2.09 ± 0.11	66.2 ± 1.3	782.6 ± 0.4	0.707807 ± 26
G4-III[a]	44	1000	1.164 ± 0.004	1.86 ± 0.07	1074.0 ± 16.1	454.1 ± 0.3	0.707679 ± 23
Soil leachate	0	0	0.986 ± 0.005	1.87 ± 0.08	32527 ± 1395	177.1 ± 0.1	—

[a] Samples not located on the main flow direction.
[b] Calculated along a flow line from the catchment divide.

Table 3
U-series and Sr isotope data for the solid samples

Sample	Sample elevation (m)	Sample depth (m)	Mean water-table depth (m)	Residue[a] (wt%)	($^{234}U/^{238}U$)	($^{230}Th/^{232}Th$)	($^{238}U/^{232}Th$)	($^{230}Th/^{234}U$)	U (ng g^{-1})	Th (ng g^{-1})	$^{87}Sr/^{86}Sr$
Outcrop chalk	140	0	45	2.39	0.878 ± 0.004	3.80 ± 0.07					
R1_10_1	192	10	44	3.36	0.987 ± 0.002	2.85 ± 0.01	2.52 ± 0.03		492.3 ± 0.3		0.707511 ± 11
R1_40_2	162	40	44	6.14	1.005 ± 0.004	6.05 ± 0.05	3.03 ± 0.01	1.99 ± 0.02	882.5 ± 0.4	883.3 ± 1 7	0.707488 ± 13
R1_49_2	153	49	44	9.54	1.002 ± 0.005	3.42 ± 0.13	2.51 ± 0.06	1.35 ± 0.05	399 ± 0.2	481.9 ± 5.8	0.707502 ± 16
R2_24	120	24	42		0.982 ± 0.012	3.51 ± 0.07	3.13 ± 0.01	1.14 ± 0.03	497 5 ± 0 7	481 7 ± 0 3	0.707483 ± 14
R2_34	110	34	42		1.059 ± 0.006	6.03 ± 0.08	5.06 ± 0.02	1.12 ± 0.02	451.2 ± 0.3	270.3 ± 0 5	0.707518 ± 15
R2_44	100	44	42		1.019 ± 0.006	5.50 ± 0.03	5.11 ± 0.01	1.06 ± 0.01	519.8 ± 0.4	308.5 ± 0 1	0.707437 ± 16
R2_53	91	53	42	2.03	1.109 ± 0.102	8.03 ± 0.04	5.37 ± 0.13	1.35 ± 0.13	457.3 ± 5.3	258.4 ± 0 1	0.707451 ± 14
R2_64	80	64	42	0.84	1.010 ± 0.013	4.88 ± 0.05	4.81 ± 0.12	1.00 ± 0.02	560.9 ± 0.7	353.8 ± 0 2	0.707487 ± 13
R2_74	69	74	42	0.84	1.039 ± 0.003	10.77 ± 0.15	7.39 ± 0.42	1.40 ± 0.08	539.9 ± 0.4	104.2 ± 0.8	0.707416 ± 13
R3_15_2	218	15	36	3.50	0.982 ± 0.003	2.97 ± 0.01					0.707526 ± 11
R3_36_1	197	36	36		1.037 ± 0.017	3.66 ± 0.13	3.09 ± 0.06	1.14 ± 0.05	568.6 ± 1.3	557.5 ± 5.6	
R3_36_2	197	36	36	4.26	1.029 ± 0.027	3.55 ± 0.11	3.10 ± 0.05	1.11 ± 0.05	570.6 ± 2	558.5 ± 4.2	0.707482 ± 12
R3_36_3	197	36	36		1.037 ± 0.004	3.71 ± 0.12	3.24 ± 0.04	1.10 ± 0.04	595.7 ± 0.2	557.5 ± 3.8	
R3_45_1	188	45	36	6.43	0.960 ± 0.010	2.00 ± 0.06	1.42 ± 0.01	1.47 ± 0.05	428.9 ± 0.5	917.6 ± 3.3	0.707525 ± 13
R3_45_2	188	45	36	8.84	1.013 ± 0.007	1.97 ± 0.06	1.46 ± 0.01	1.31 ± 0.04	405.7 ± 0.3	843.7 ± 3.1	
R4_15_1	218	15	29		1.006 ± 0.005	3.2 ± 0.12	2.69 ± 0.01	1.19 ± 0.04	473.7 ± 0.3	534.9 ± 1.2	0.707536 ± 12
R4_15_3	218	15	29	4.97	1.012 ± 0.004						
R4_25_1	208	25	29	11.98	0.970 ± 0.004	4.02 ± 0.06	3.88 ± 0.01	1.07 ± 0.02	721 ± 0.3	564.3 ± 0.6	0.70752 ± 21
R4_41_1	192	41	29	2.89	1.013 ± 0.010	5.68 ± 0.18	5.04 ± 0.07	1.11 ± 0.04	821.4 ± 1.1	494.8 ± 3.9	0.707519 ± 10
R4_41_2	192	41	29		1.064 ± 0.016	5.03 ± 0.16	4.21 ± 0.07	1.12 ± 0.04	655.8 ± 1.3	472.1 ± 3.8	
R5_24	172	24	25	11.48	0.915 ± 0.008	5.33 ± 0.04	2.75 ± 0.01	2.12 ± 0.02	520 ± 0.6	573.0 ± 0.4	0.707524 ± 11
R5_34	162	34	25	3.65	0.896 ± 0.003	4.91 ± 0.05	4.66 ± 0.01	1.14 ± 0.01	546.7 ± 0.1	344.5 ± 2.3	0.707467 ± 14
R5_44	152	44	25	4.82	1.015 ± 0.010				567 ± 0.7		0.707527 ± 11
R5_53	143	53	25		0.993 ± 0.007	6.90 ± 0.04	6.47 ± 0.01	1.07 ± 0.01	673.5 ± 0.6	315.6 ± 0.1	0.707462 ± 13
Fracture wall R4	183	13	29	22.73	1.000 ± 0.002	1.89 ± 0.01	1.79 ± 0.01	0.97 ± 0.01	1148 ± 0.7	1987.0 ± 12	

[a] Residue after acetic acid dissolution.

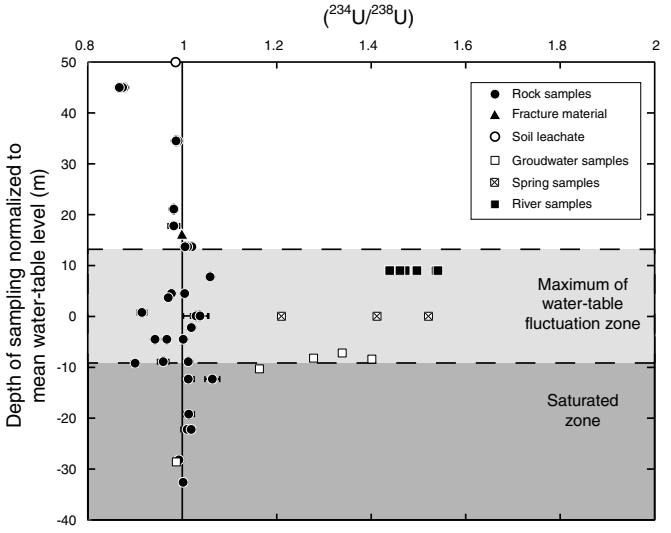

Fig. 2. Plot of ($^{234}U/^{238}U$) activity ratios measured in solid and aqueous phases versus depth of sampling calculated relative to the mean water-table level in each well. The dark vertical line represents secular equilibrium. The solid circles represent rock samples from drilling cores, the triangle represent fracture material, and the open, crossed and solid squares represent groundwater, spring-water and river-water samples, respectively. The open circle represents the soil leachate that is indicated above the aquifer, with no relation to the height above the water table. Water samples show enrichment in ^{234}U whereas rock samples show contrasted values with ^{234}U depletion mainly in the upper part of the aquifer and enrichment in the water-table fluctuation zone and in the saturated zone of the aquifer.

zone results in ($^{234}U/^{238}U$) > 1 in the water samples and ^{234}U depletion in the chalk. Remarkably, ($^{234}U/^{238}U$) > 1 are found in rock samples from the zone of water-table fluctuation (Fig. 2). The simplest explanation for ($^{234}U/^{238}U$) > 1 is that ^{234}U-rich material has been deposited in these layers. We consider *a priori* two possible mechanisms for U deposition: (1) a redox front due to seasonal

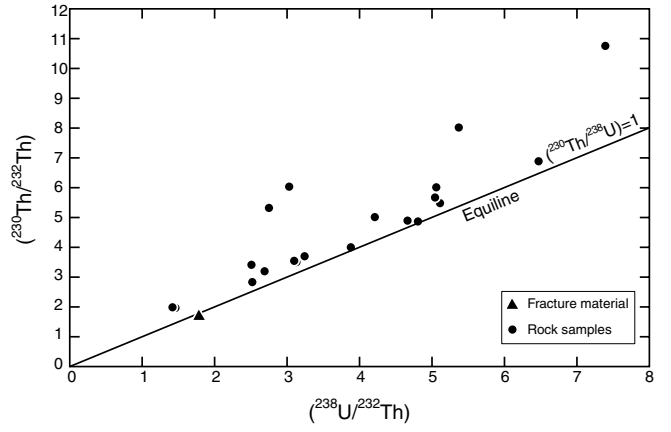

Fig. 3. ($^{230}Th/^{232}Th$) versus ($^{238}U/^{232}Th$) activity ratios in core samples for the different boreholes. The equiline is the line of secular equilibrium. The triangle and circles represent the fracture material and the rock samples, respectively. All samples plot above the line of secular equilibrium and show a wide range of ($^{238}U/^{232}Th$) activity ratios. They all show preferential U leaching from rock.

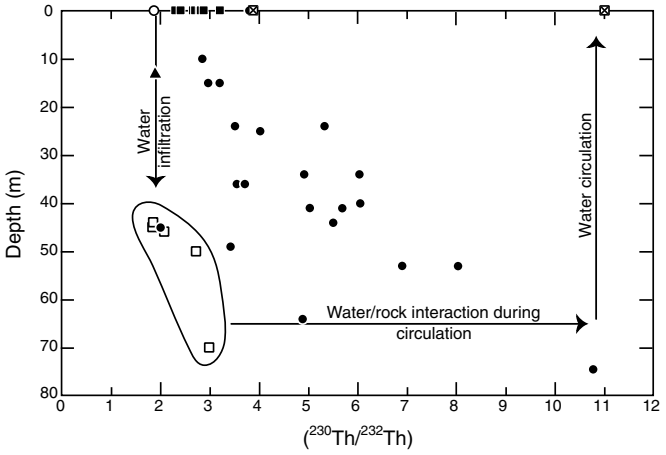

Fig. 4. Plot of ($^{230}Th/^{232}Th$) versus depth of sampling for rocks (solid circles), fracture material (triangles), soil leachate (open circle), groundwater (open squares), spring (crossed squares) and river (solid square) samples. Groundwaters are characterized by ($^{230}Th/^{232}Th$) activity ratios lower than rock samples. The arrows represent a possible evolution line for ($^{230}Th/^{232}Th$) during water circulation.

changes in the aquifer or (2) precipitation of calcite due to variation in its saturation index. No significant difference has been observed in the water oxidation state (Table 2) measured in situ during high flow (March) and low flow (September–October) regimes. In contrast, there seems to be difference in calcite saturation index ($\Omega_{calcite}$, Table 1), between the two periods. In high water flow regime, groundwater samples have $\Omega_{calcite}$ between −5.1 and −0.43, indicating undersaturation with respect to calcite, compared to values of −0.26 and 0.04 in the low water flow regime, indicating a slight undersaturation or saturation. This can promote precipitation of calcite during the low water flow regime, which can result in ($^{234}U/^{238}U$) > 1 in the chalk samples located in the water-table oscillation zone. As water oxidation state has not been measured for the entire annual cycle, more data about redox state would be useful to be fully conclusive.

In contrast with the ^{234}U–^{238}U system, ^{230}Th–^{238}U systematics in rocks shows that U is depleted relative to more immobile Th. From the ($^{230}Th/^{232}Th$)/($^{238}U/^{232}Th$) ratios, it is clear that all the rock samples are characterized by ($^{230}Th/^{238}U$) greater than 1 (Fig. 3). The trend in Fig. 3 could result from a heterogeneous aquifer matrix with variable initial compositions (Fig. 5a) that evolves away from the equiline (line of secular equilibrium in Fig. 3) as U is being leached. The digestion of the rock samples reveals that the matrix is not composed of pure calcium carbonate. There is a residual phase after digestion with acetic acid amounting between 0.8 and 12 wt% of the total sample (Table 3). Therefore, the chalk is not a completely homogeneous lithology and the trend in Figs. 3 and 5a is inferred to result from variable composition in ($^{238}U/^{232}Th$). Sr isotope ratios are correlated with ($^{230}Th/^{232}Th$) (Fig. 6), which can be interpreted in terms of a mixing line between a carbonate endmember (high U/Th, low $^{87}Sr/^{86}Sr$) and a

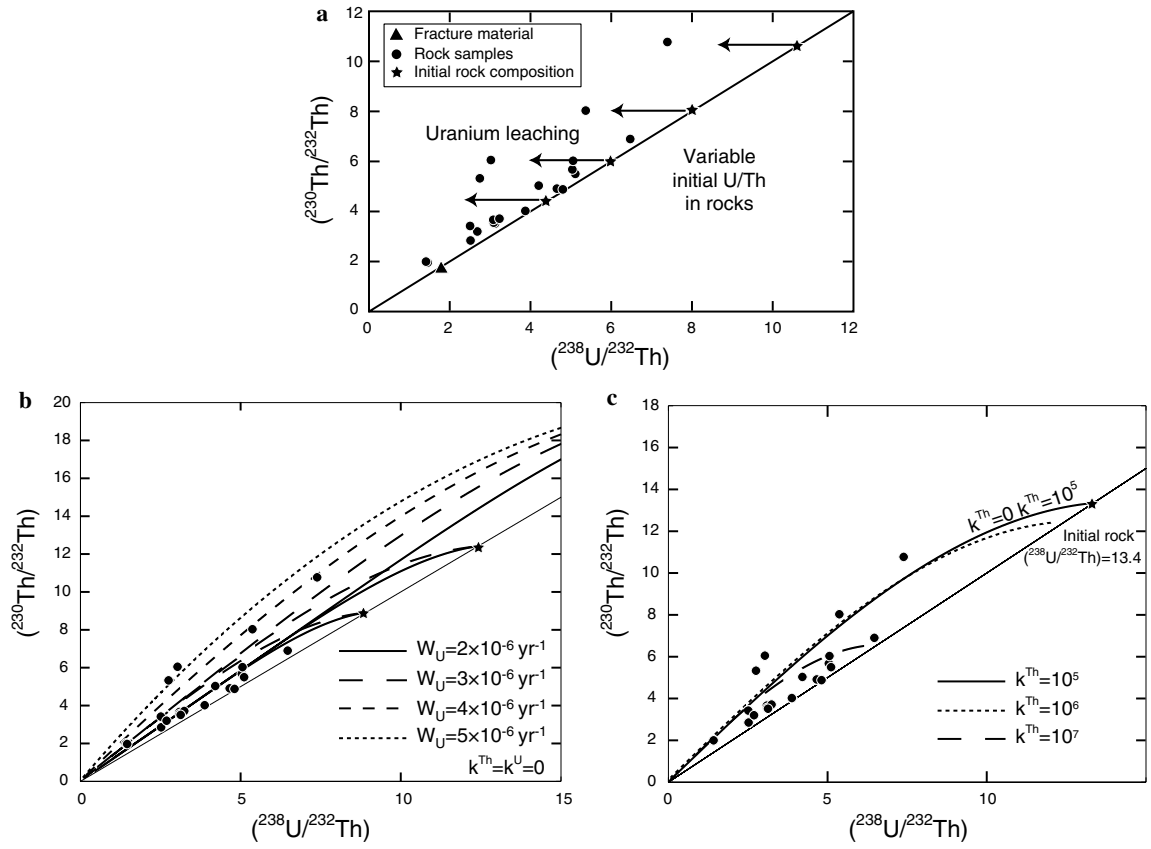

Fig. 5. Different scenarios for U leaching in rock samples. (a) Initial rock composition with a wide range evolving as uranium is being leached, (b) plot with model curves showing the evolution of (^{230}Th/^{232}Th) versus (^{238}U/^{232}Th) in the bulk solid phase without adsorption ($k^{Th} = k^{U} = 0$) for various initial rock compositions and U weathering rate, and (c) plot with model curves showing the evolution of (^{230}Th/^{232}Th) versus (^{238}U/^{232}Th) in the bulk solid phase (solid and surface layer) for $W_U = 3 \times 10^{-6}$ yr^{-1}, $k^U = 750$ and initial rock composition of (^{238}U/^{232}Th) = 13.4 and k^{Th} of 0, 10^5, 10^6 and 10^7.

silicate endmember (low U/Th, high ^{87}Sr/^{86}Sr). The Sr isotope ratios vary positively with the mass fraction of acid-insoluble residue (Table 3). However, there is no relationship between the bulk Th concentration and the residue fraction. The residual phase has been characterized by X-ray diffraction at LGIT (Laboratoire de Géophysique Interne et Tectonophysique, Grenoble) and it is predominantly silicates (mainly quartz and kaolinite). Thorium is mainly contained in this silicate phase and is obviously less mobilized than U during weathering.

Groundwaters have (^{230}Th/^{232}Th) ratios lower than the chalk samples but similar to the soil leachate and the fracture material (Fig. 4). As shown in Fig. 7 (^{230}Th/^{232}Th) in water samples tends to increase with the distance from the catchment divide. The water collected near the recharge mostly results from vertical infiltration through the soil and the vadose zone and has not flowed over a long distance within the saturated part of the aquifer and has therefore not interacted for a long time with the chalk matrix. It can be inferred that increasing water/rock interaction tends to increase (^{230}Th/^{232}Th). All the water samples show a more radiogenic signature in ^{87}Sr/^{86}Sr (Fig. 6) than the rock samples. The surface layers, where rainwaters infiltrate, are richer in silicates (with a low ^{230}Th/^{232}Th) than the deeper part of aquifer matrix (chalk with a high

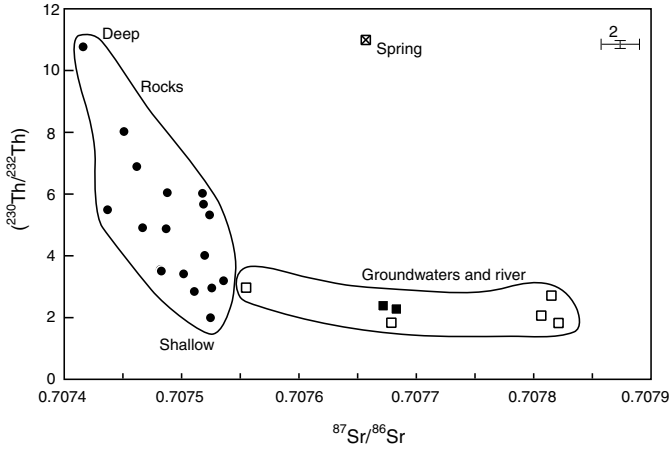

Fig. 6. Plot of (^{230}Th/^{232}Th) activity ratios versus ^{87}Sr/^{86}Sr for rock and water samples. The solid circles represent rock samples from drill cores, the open, crossed and solid squares represent groundwater, spring and river samples, respectively. The relationship between Th and Sr isotope systems in rocks shows that (^{230}Th/^{232}Th) ratios are linked to lithological variations. The deep rock samples are richer in carbonate phase than shallow samples which show also more radiogenic ^{87}Sr/^{86}Sr. Water samples show more radiogenic ^{87}Sr/^{86}Sr ratios than rocks, indicating that they have circulated in a medium richer in silicates (probably clays from soil) than the aquifer rocks.

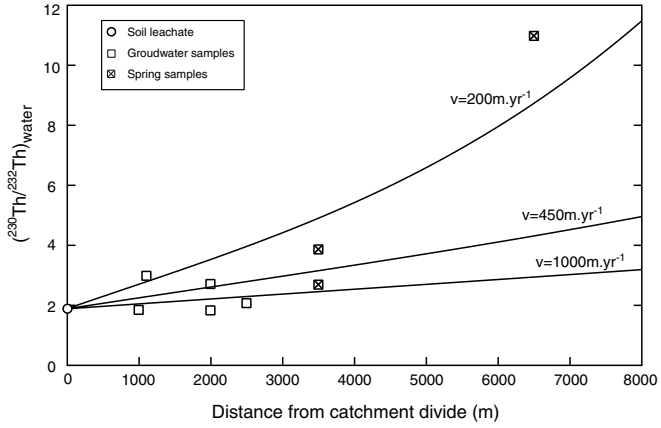

Fig. 7. (^{230}Th/^{232}Th) activity ratios versus distance from the catchment divide in groundwater (open square) and spring (crossed square) samples. Activity ratio for soil leachate (open circle) is set at a distance of zero. The data show that (^{230}Th/^{232}Th) activity ratios in water increase with distance from the watershed divide. Starting from an initial (^{230}Th/^{232}Th) activity ratio in infiltrating water (as given by the soil leachate), the curves represent the predicted behavior of (^{230}Th/^{232}Th) in water versus distance from the catchment divide for an age of 1 Myr. Curves are labeled with water flow velocities (v). This range of water flow velocity is consistent with hydrogeological modeling for this aquifer (F. Renard, pers. comm.).

^{230}Th/^{232}Th). Thus, it is likely that the Th isotope signature of water is inherited from the upper part of the vadose zone. The possible source of radiogenic Sr and radionuclides in groundwater may also be the soil. As listed in Table 2, soil leachate has a (^{230}Th/^{232}Th) ratio of 1.87, which is similar to the lowest groundwater values. The coating of the fracture sample could reflect the same Th isotope signature as the soil and further suggests that fractures represent a rapid pathway of water infiltration from the recharge area. Moreover, the Th concentration measured in groundwater samples largely exceeds its solubility based on the major ion composition of the water, using the geochemical code CHESS (van der Lee and De Windt, 2002). A logical inference is that Th is bound to colloids when infiltrating from the soils to the aquifer, which increases the *apparent* solubility of Th (Langmuir and Herman, 1980). Studies have shown that organic colloids promote the transport of radionuclides in river waters (Porcelli et al., 1997, 2001; Viers et al., 1997), and that Th is strongly complexed by humic acid and products resulting from humic acid decomposition (Cacheris and Choppin, 1987; Viers et al., 1997). The analyses of dissolved organic carbon (DOC) show no detectable trace of organic carbon in the samples (<1 mg L^{-1}). Although we have not identified the carrier of Th in the chalk aquifer waters, colloids seem to be a very likely candidate for explaining the enhanced Th transport.

5. Quantifying U-series transport processes within the aquifer

An important aim of this study is to quantify the processes that control radionuclide migration at the water/rock interface. Previous studies based primarily on measurements in the water phase have highlighted the application of U-series disequilibria to quantify parameters influencing radionuclide mobility (Krishnaswami et al., 1982; Luo et al., 2000; Tricca et al., 2000, 2001; Reynolds et al., 2003). Many of these studies consider that the U-series decay chain is in secular equilibrium in the solid phase. U-series disequilibria in the bulk solid phase result from protracted periods of weathering and the precise determination of the U-series isotope distribution in the solid phase provides constraints on weathering rates. Our data set includes analyses of both the solid and water phases of the aquifer that enables us to construct a complete mass-balance calculation that has not been possible in other studies of U-series in aquifer systems. Furthermore, it enables us to compare sorption coefficients measured in the laboratory with our field determinations which integrate a much larger scale.

5.1. Basic concept of the model

The model described below is a one-dimensional time-dependent model for the migration of U-series nuclides in a porous medium. Similar to previous modeling attempts (Tricca et al., 2000, 2001; Keum and Hahn, 2003; Reynolds et al., 2003), it takes into account three phases: (1) a solid phase that does not directly exchange with the water phase, (2) a surface layer that represents the part of the solid phase accessible to liquid phase (where physico-chemical reactions, such as adsorption/desorption, take place), and (3) a liquid phase.

The processes that affect the distribution of nuclides in the different phases are: (a) in situ production by decay of the parent nuclide, (b) in situ decay of the nuclide, (c) α-recoil which ejects a fraction of the daughter nuclide produced from solid to liquid phase, (d) dissolution/precipitation of the solid phase with a first-order rate specific to each element, (e) adsorption of nuclides from the liquid phase onto the surface layer, (f) desorption of nuclides from the surface layer to the liquid phase. U oxidation state is usually an important parameter to assess its mobility but, as shown in Sections 3 and 4, this parameter is not crucial in the chalk aquifer due to oxidizing conditions.

Several models have been developed to quantify the behavior of radionuclides in groundwater (Krishnaswami et al., 1982; Luo et al., 2000; Tricca et al., 2001) and have all used a similar approach: they all considered aquifer phases to be at steady state and neglected the possible time-evolution of the solid phase. Our data clearly show that the solid is not in secular equilibrium with respect to U-series nuclides: this indicates that U-series fractionation is recent (less than 300 kyr). As a consequence, we have considered the time dependence of radionuclides both in the liquid and solid phases. However, similarly to other studies, the surface layer is considered to be in quasi-steady state (Tricca et al., 2000, 2001). In fact, as the exchange between the water and

the surface layer is fast, the surface layer always remains in quasi-equilibrium with the water.

We consider an elementary volume of aquifer and the mass conservation equation for a given radionuclide i in the solid phase is:

$$\frac{\partial \rho_s(1-\Phi)(1-f_{sl})C_s^i}{\partial t} = \rho_s(1-\Phi)(1-f_{sl})(1-\varepsilon_i)\lambda_p C_s^p + \frac{1}{2}\rho_{sl}(1-\Phi)f_{sl}\varepsilon_i'\lambda_p C_{sl}^p - \rho_s(1-\Phi)(1-f_{sl})(\lambda_i + W_i)C_s^i, \quad (1)$$

where C is the nuclide concentration in mol per kg, s and sl subscript refer to solid phase and surface layer, respectively, i and p superscripts denote the nuclide and its parent, respectively, λ is the decay constant (yr^{-1}), Φ is the porosity of the aquifer, f_{sl} is the volume of surface layer per volume of solid phase, ε_i is the fraction of nuclide i ejected into the liquid phase from the solid, ε_i' is the fraction of nuclide i ejected into either the solid or the liquid phase from the surface layer, ρ is the density of a given phase ($kg\,m^{-3}$) and W_i is the weathering rate of element i (yr^{-1}). The values of the parameters that are typical for the chalk aquifer are listed in Table 4.

The sources of nuclides in the rock are in situ decay of the parent nuclide (first term in the right-hand side (RHS) of Eq. (1)) and recoil from the surface layer (second term in the RHS of Eq. (1)). We consider that half of the fraction recoiling from the surface layer goes to the solid phase and the other half goes to the liquid phase. Nuclides are released from the solid phase to the water phase through recoil and weathering (third term in RHS of Eq. (1)) and they decay in situ to their daughter nuclide (third term in RHS of Eq. (1)). The conservation equation of nuclide i in the liquid phase can be written as follows:

$$\frac{\partial \rho_w \Phi C_w^i}{\partial t} = -v\frac{\partial \rho_w \Phi C_w^i}{\partial x} + \rho_s(1-\Phi)(1-f_{sl})W_i C_s^i + \rho_s(1-\Phi)(1-f_{sl})\varepsilon_i\lambda_p C_s^p + \rho_{sl}(1-\Phi)k_{-1}^i S C_{sl}^i + \frac{1}{2}\rho_{sl}(1-\Phi)f_{sl}\varepsilon_i'\lambda_p C_{sl}^p + \rho_w\Phi\lambda_p C_w^p - \rho_w\Phi\lambda_i C_w^i - \rho_w(1-\Phi)k_1^i S C_w^i, \quad (2)$$

where w subscript refers to water phase, v is the water velocity ($m\,yr^{-1}$), k_1^i and k_{-1}^i represent the adsorption and desorption rates, respectively ($m\,yr^{-1}$) and S is the area of surface layer per volume of rock ($m^2\,m^{-3}$).

In Eq. (2), the nuclide concentration in water evolves as a function of both time and distance from the water divide. The advective term is controlled by the water velocity (first term in RHS of Eq. (2)). Nuclides are produced in the liquid phase by in situ decay of parent isotopes (sixth term in RHS of Eq. (2)). They are released from the solid to the water phase by weathering (second term in RHS of Eq. (2)) and α-recoil (third term of RHS in Eq. (2)), from the surface layer by α-recoil (fifth term in RHS of Eq. (2)) and desorption (fourth term in RHS of Eq. (2)). The sink term for nuclides in the liquid phase are in situ decay (seventh term in RHS of Eq. (2)) and adsorption onto the surface layer (eighth term in RHS of Eq. (2)). The conservation equation for nuclide i in the surface layer is as follows:

Table 4
Model parameters

Symbol	Parameters	Value	Unit
ρ_s [a]	Rock density	2700	$kg\,m^{-3}$ of rock
ρ_{sl} [a]	Surface layer density	2700	$kg\,m^{-3}$of surface layer
ρ_w [a]	Water density	1000	$kg\,m^{-3}$ of water
Φ [b]	Porosity	0.4	
r [a]	Chalk grain radius	0.38×10^{-6}	m
v [*]	Water flow velocity	450	$m\,yr^{-1}$
T [c]	Thickness of surface layer	1–1.5	nm
S [*]	Surface of surface layer per volume of solid	8×10^{6}	m^{-1}
f_{sl} [*]	Volume of surface layer per volume of solid	$8–12\times10^{-3}$	
W_U [*]	Uranium weathering rate	$2–5\times10^{-6}$	yr^{-1}
W_{Th} [*]	Thorium weathering rate	1×10^{-9}	yr^{-1}
$\varepsilon_{^{234}Th}$ [*]	Fraction of recoil ^{234}Th from the rock phase	0.05	
$\varepsilon_{^{230}Th}$ [*]	Fraction of recoil ^{230}Th from the rock phase	0.06	
ε_i' [*]	Fraction of recoil nuclide i from the surface layer	1	
k^{U*}	Uranium distribution coefficient	500–1000	
k^{Th*}	Thorium distribution coefficient	$1–10\times10^{5}$	
C_n^i	Concentration of nuclide i in the phase n		$mol\,kg^{-1}$ of phase

[a] Vachier et al. (1979).
[b] Crampon et al. (1993a).
[c] Doyle et al. (2004).
[*] Calculated in this study.

$$\frac{\partial \rho_{sl}(1-\Phi)f_{sl}C^{i}_{sl}}{\partial t} = \rho_w(1-\Phi)k^{i}_{1}SC^{i}_{w} + \rho_{sl}(1-\Phi)f_{sl}(1-\varepsilon'_{i})\lambda_{p}C^{p}_{sl} - \rho_{sl}(1-\Phi)k^{i}_{-1}SC^{i}_{sl} - \rho_{sl}(1-\Phi)f_{sl}\lambda_{i}C^{i}_{sl}. \quad (3)$$

Both adsorption and desorption affect the surface layer composition. We consider that nearly all the nuclides produced by α-decay recoil from this layer are lost, with half being ejected into the solid and the other half into the water phase. This surface layer is assumed to be in steady state such that:

$$C^{i}_{sl} = \frac{\rho_w k^{i}_{1} S}{\rho_{sl}(k^{i}_{-1}S + f_{sl}\lambda_{i})}C^{i}_{w} + \frac{f_{sl}\lambda_{p}(1-\varepsilon'_{i})}{k^{i}_{-1}S + f_{sl}\lambda_{i}}C^{p}_{sl}. \quad (4)$$

The surface layer thickness (T), the surface area (S) and the volume of this layer (f_{sl}) are not independent parameters. The surface S (Eq. (5)) is defined as the surface area of the surface layer divided by the volume of the grain:

$$S = \frac{4\pi r^2}{\frac{4}{3}\pi(r-T)^3} = \frac{3r^2}{(r-T)^3}. \quad (5)$$

with r the average grain radius. T ranges from 1 to 1.5 nm according to Doyle et al. (2004), and represents 0.25–0.4% of the grain radius (380 nm according to Vachier et al. (1979)). Thus, T has little influence on the estimate of S and can be neglected in Eq. (5). The fraction of solid volume occupied by the surface layer is defined as follows:

$$f_{sl} = 1 - \left(\frac{r-T}{r}\right)^3 \approx \frac{3T}{r}. \quad (6)$$

Eq. (1) was solved by standard methods for first-order ordinary differential equation while an analytical solution was obtained for Eq. (2) by Laplace transform methods. Decay constants were taken from Bourdon et al. (2003) with $\lambda_{^{238}U} = 1.551\times10^{-10}\ yr^{-1}$, $\lambda_{^{234}Th} = 10.505\ yr^{-1}$, $\lambda_{^{234}U} = 2.823\times10^{-6}\ yr^{-1}$, $\lambda_{^{230}Th} = 9.158\times10^{-6}\ yr^{-1}$ and $\lambda_{^{232}Th} = 4.916\times10^{-11}\ yr^{-1}$. For the initial conditions at $t=0$, the rock was taken to be in secular equilibrium, and for the boundary conditions at $x=0$, the composition of the water at the recharge was similar to the composition of the soil leachate (see Table 2). Solution of the equations for each radionuclides, in groundwater and rock, is too long to be written in this paper and is given in Hubert (2005).

5.2. Transport mechanisms of U and Th

5.2.1. The role of adsorption/desorption and dissolution on U/Th fractionation

We have considered *a priori* that the water flow in the chalk aquifer has lasted between 10 ka and a few Ma. The U-series data for rock samples reported in Table 3 represent bulk rock analysis where the surface layer has not been isolated. As a consequence, in order to compare the modeling results with our observations, we calculated the bulk solid composition which integrates the solid phase (s) and the surface layer (sl) as calculated in the model. In what follows, we used the model results to estimate the rate parameters characterizing dissolution (W), adsorption and desorption (k's).

Dissolution affects the bulk solid composition while adsorption and desorption affect the surface layer. For example, the evolution of ^{238}U in the solid phase depends on the weathering rate and the initial U concentration ($C^{^{238}U}_{st0}$) and can be expressed as:

$$C^{^{238}U}_{s} = C^{^{238}U}_{st0}\,e^{-W_U t}. \quad (7)$$

In contrast, the evolution of ^{238}U in the surface layer depends on surface phenomena:

$$C^{^{238}U}_{sl} = \frac{\rho_w k^{U}_{1} S}{(\rho_{sl}k^{U}_{-1}S + f_{sl}\lambda_{^{238}U})}C^{^{238}U}_{w}. \quad (8)$$

In Eq. (8), $f_{sl}\lambda_{^{238}U}$ can be neglected, so it follows that:

$$C^{^{238}U}_{sl} = \frac{\rho_w k^{U}_{1} S}{\rho_{sl}k^{U}_{-1}S}C^{^{238}U}_{w} = \frac{\rho_w}{\rho_{sl}}k^{U}C^{^{238}U}_{w}, \quad (9)$$

where k^U is a dimensionless U distribution coefficient defined as the ratio of the adsorption/desorption rate constants. $C^{^{238}U}_{w}$, the concentration of ^{238}U in the water phase, is given by the following equation:

$$C^{^{238}U}_{w} = C^{^{238}U}_{wx0} + \frac{\rho_s(1-\Phi)(1-f_{sl})}{\rho_w\Phi}C^{^{238}U}_{st0}\left(e^{-W_U(t-x/v)} - e^{-W_U t}\right). \quad (10)$$

After algebraic manipulation of Eq. (9), the adsorption terms (fourth and eighth term in the RHS of Eq. (2)) disappear. The ^{238}U concentration in the water increases only due to weathering. The U adsorption onto the surface layer is assumed to be in steady state (see above) and the variation of ^{238}U concentration in the water through time is not influenced by this process.

The equations describing the evolution of ^{232}Th concentration in the solid and surface layer are similar to Eqs. (7)–(10), with parameters $\lambda_{^{232}Th}$, W_{Th} and k^{Th}.

We first attempt to determine the values of W_U and W_{Th} by assuming that adsorption is negligible ($k^U = k^{Th} = 0$). In this context, the ^{230}Th–^{238}U fractionation shown in Fig. 3 requires that $W_U > W_{Th}$, which implicitly means that dissolution is not congruent. The combined Th and Sr clearly demonstrate that the initial U/Th ratios in the solids are not constant. In order to model the data shown in Fig. 3, we have assumed a variation in initial $^{238}U/^{232}Th$ ratios. Model parameters were adjusted by trial and error in order to fit the collected data for both water and rock samples. ($^{238}U/^{232}Th$) is changing through time, and for $W_U \geqslant 7W_{Th}$ the time evolution is independent of the value of W_{Th}. The data shown in Fig. 5b can be explained for W_U ranging between 2×10^{-6} and $5\times10^{-6}\ yr^{-1}$. Previous studies of U-series disequilibria in continental environ-

ments have derived a similar parameter, which was denominated as a leaching coefficient, weathering rate or dissolution rate constant (Tricca et al., 2001; Vigier et al., 2001, 2005; Maher et al., 2004; Dosseto et al., 2006). This parameter was assumed to be a first-order rate constant, with values ranging from 10^{-8} to 10^{-5} yr^{-1} for U and from 10^{-13} to 10^{-7} yr^{-1} for Th weathering from a variety of lithologies (mainly sedimentary or basaltic lithologies but not chalk).

We then test whether adsorption/desorption on the surface layer could play a role in the data shown in Fig. 3, which means the surface layer is not negligible. As shown in Fig. 5c, for k^{Th} ranging between 10^5 and 10^6, a slight effect can be seen, but for k^{Th} ranging between 0 and 10^5 there is hardly any effect of the surface layer on the Th budget of the bulk solid. This is due to the small volume of the surface layer relative to the grain. Values of $k^{Th} < 10^5$ yield incoherent value for ($^{230}Th/^{232}Th$) in water (<0), and $k^{Th} > 10^6$ cannot explain the solid phase data. Thus, k^{Th} has been estimated to range between 10^5 and 10^6.

For the determination of k^U values, we used the variation of ($^{234}U/^{238}U$) in water versus the distance from the catchment divide for various water flow velocities (Fig. 8). Considering a heterogeneous water flow, due to the hydrologic properties of the chalk (Price et al., 1993), k^U has been estimated to range between 500 and 1000. With this range of values, our calculations could not detect any effect of k^U on the U behavior in the solid phase. This is attributed again to the small volume of the surface layer relative to the grain. Overall, the adsorption phenomenon on U and Th cannot be responsible for the variation of ($^{230}Th/^{238}U$) in the solid phase and can therefore be neglected in studies of carbonate chemical weathering.

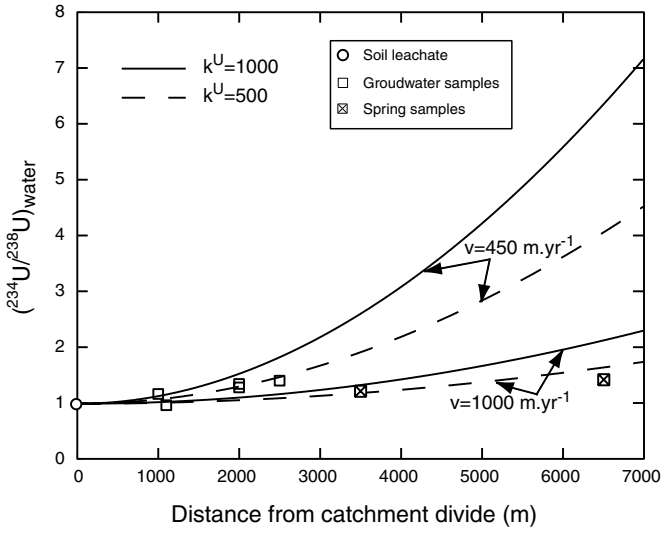

Fig. 8. Predicted behavior of ($^{234}U/^{238}U$) in the aquifer water versus distance from the catchment divide for various k^U and water flow velocities compared with groundwater (open square) and spring (crossed square) samples.

5.2.2. Effect of α-recoil on ^{234}U and ^{230}Th mobilization

As ^{238}U decays in the chalk, a fraction of daughter ^{234}Th is ejected in the water phase due to α-recoil (Kigoshi, 1971). This results in substantial mobilization of ^{234}Th and ^{230}Th in the water. To estimate the magnitude of this effect, however, the fraction of recoiled nuclide $\varepsilon_{^{234}Th}$ must be estimated using ($^{234}U/^{238}U$) in the rock. In fact, the fractionation observed between ^{234}U and ^{238}U must be the result of ^{238}U–^{234}Th fractionation by α-recoil, as both ^{234}Pa and ^{234}U are being produced by β-decay that does not produce a substantial recoil effect. The parameter $\varepsilon_{^{234}Th}$ also integrates the preferential leaching of ^{234}U due to damage caused to the crystal lattice by ^{234}Th α-decay. The time evolution of ^{234}Th and ^{234}U nuclides concentration in the solid phase can be written as follows:

$$C_s^{^{234}Th} = (1-\varepsilon_{^{234}Th})\left(\frac{\lambda_{^{238}U}}{\lambda_{^{234}Th}}\right)C_{st0}^{^{238}U}(e^{-W_U t} - e^{-\lambda_{^{234}Th} t}) + C_{st0}^{^{234}Th} e^{-\lambda_{^{234}Th} t}, \quad (11)$$

$$C_s^{^{234}U} = \frac{\lambda_{^{234}Th}\lambda_{^{238}U}(1-\varepsilon_{^{234}Th})C_{st0}^{^{238}U}}{\lambda_{^{234}U}(\lambda_{^{234}Th} - W_U)}(e^{-W_U t} - e^{-(\lambda_{^{234}U}+W_U)t}) + C_{st0}^{^{234}U} e^{-(\lambda_{^{234}U}+W_U)t}. \quad (12)$$

For $t > 5T_{^{234}Th}$, with $T_{^{234}Th}$ being the half-life of ^{234}Th, $e^{-\lambda_{^{234}Th} t}$ can be neglected in Eq. (11), and ($^{234}Th/^{238}U$) of the chalk is given by the following equation:

$$(^{234}Th/^{238}U)_s = (1-\varepsilon_{^{234}Th}). \quad (13)$$

This activity ratio reaches a constant value almost instantaneously. As seen above, $\lambda_{^{234}U}$ and W_U are of the same order of magnitude, but $W_U \ll \lambda_{^{234}Th}$. The activity ratio of ($^{234}U/^{238}U$) in the solid phase can thus be expressed as:

$$(^{234}U/^{238}U)_s = (1-\varepsilon_{^{234}Th})(1-e^{-\lambda_{^{234}U} t}) + \frac{\lambda_{^{234}U} C_{st0}^{^{234}U}}{\lambda_{^{238}U} C_{st0}^{^{238}U}} e^{-\lambda_{^{234}U} t}. \quad (14)$$

If the solid phase is considered to be in secular equilibrium at $t = 0$, the second term of Eq. (14) can be simplified as follows:

$$(^{234}U/^{238}U)_s = (1-\varepsilon_{^{234}Th})(1-e^{-\lambda_{^{234}U} t}) + e^{-\lambda_{^{234}U} t}. \quad (15)$$

Eqs. (13) and (15) illustrate the importance of α-recoil effect on the behavior of ^{234}Th and ^{234}U in the solid phase. Fig. 9 shows model calculations of ($^{234}U/^{238}U$) as a function of time for various α-recoil fractions. As expected, with increasing $\varepsilon_{^{234}Th}$, there is a marked decrease in ($^{234}U/^{238}U$) in the solid. The measured chalk ($^{234}U/^{238}U$) show contrasting values between the various sections of the aquifer (saturated zone, water-table oscillation zone or unsaturated zone; see Section 3). In our model, weathering does not generate fractionation between ^{234}U and ^{238}U. Water infiltrating at the top of the aquifer is in equilibrium with the soil P_{CO_2}, which means that calcite precipitation is unlikely in this context. Thus, the observed depletion in ^{234}U relative to ^{238}U is entirely due to α-recoil process from

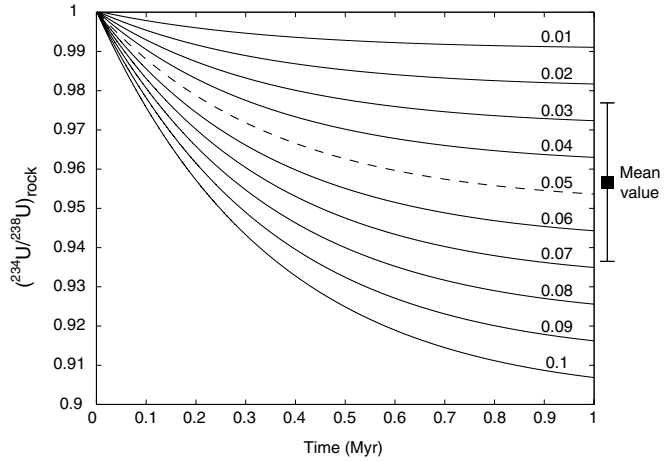

Fig. 9. Predicted behavior of (^{234}U/^{238}U) in chalk versus time scale of the aquifer age for various ^{234}Th recoil fractions. Models curves have been labeled with $\varepsilon_{^{234}\mathrm{Th}}$ values.

its parent ^{234}Th, and $\varepsilon_{^{234}\mathrm{Th}} = 0.05$ for the range of measured (^{234}U/^{238}U) in the carbonates (where precipitation has not taken place). It is worth noting that the effect of weathering from the surface layer is negligible compared with the bulk solid and it has therefore not been taken into account in the model. More specifically, the surface layer would have a contribution from weathering of $\rho_s(1-\Phi)f_{sl}W_iC^i_s$, while the contribution from the bulk solid would be $\rho_s(1-\Phi)(1-f_{sl})W_iC^i_s$. Thus, given that f_{sl} is approximately 10^{-2}, this contribution is negligible.

In contrast with $\varepsilon_{^{234}\mathrm{Th}}$, $\varepsilon_{^{230}\mathrm{Th}}$ cannot be calculated directly from measured (^{230}Th/^{234}U) activity ratios as ^{230}Th depends on several other processes such as the weathering, adsorption or desorption. However, the fraction of ^{230}Th ejected from the solid to the liquid phase through α-recoil can be estimated from $\varepsilon_{^{234}\mathrm{Th}}$ and should be of the same order of magnitude, as ^{234}Th and ^{230}Th are both produced by α-decay from a U isotope (^{238}U and ^{234}U, respectively). A slight difference between $\varepsilon_{^{234}\mathrm{Th}}$ and $\varepsilon_{^{230}\mathrm{Th}}$ stems from differences in recoil energy (Ivanovich and Harmon, 1992). The kinetic energies E^i_c for the decay of ^{234}Th and ^{230}Th are:

$$E_c^{^{234}\mathrm{Th}} = Q^{^{234}\mathrm{Th}}\frac{M_\alpha}{M_\alpha + M_{^{234}\mathrm{Th}}}, \tag{16}$$

$$E_c^{^{230}\mathrm{Th}} = Q^{^{230}\mathrm{Th}}\frac{M_\alpha}{M_\alpha + M_{^{230}\mathrm{Th}}}, \tag{17}$$

where Q^i is the total energy released during the α-decay of parent nuclide of the radionuclide i (4.184 eV for ^{238}U decay and 4.754 eV for ^{234}U decay (Ivanovich and Harmon, 1992)), M_α and M_i are the masses of the helium atom and of the nuclide i, respectively. The fraction of nuclide ejected per unit of time per unit of mass is (Bourdon et al., 2003):

$$\varepsilon_i = \rho_s(1-\Phi)\frac{r^3-(r-\delta_i)^3}{4r^3}, \tag{18}$$

where ρ_s is the density of the solid and δ_i the range of the daughter nuclide. This displacement is expressed as follows (e.g., Bourdon et al., 2003):

$$\delta_i = \frac{(M_i + M_\alpha)\left(M_\alpha E_c^i K\right)\left(Z_i^{2/3} + Z_\alpha^{2/3}\right)^{2/3}}{(M_i Z_i Z_\alpha \rho)} \tag{19}$$

with Z_i the atomic number of element i, K is a constant (6.02). Based on Eqs. (18) and (19), the fraction of ^{230}Th ejected by α-recoil can be expressed as (Henderson and Slowey, 2000):

$$\varepsilon_{^{230}\mathrm{Th}} = \frac{Q^{^{230}\mathrm{Th}} M_{^{234}\mathrm{Th}}}{Q^{^{234}\mathrm{Th}} M_{^{230}\mathrm{Th}}}\varepsilon_{^{234}\mathrm{Th}}. \tag{20}$$

A factor of 1.16 has been calculated between $\varepsilon_{^{230}\mathrm{Th}}$ and $\varepsilon_{^{234}\mathrm{Th}}$. Based on Eqs. (16)–(20), the estimated value for $\varepsilon_{^{230}\mathrm{Th}}$ is 0.06, which is slightly higher than $\varepsilon_{^{234}\mathrm{Th}}$ (Table 4).

5.2.3. Length and time scales of radionuclides' transport

Some of the processes that have been described above act as retarding processes for the migration of radionuclides in the aquifer. A retardation factor represents the velocity of each nuclide relative to the water velocity in the aquifer. This can be calculated as in Krishnaswami et al. (1982) and Ku et al. (1992) using the following equation:

$$R_f^i = \frac{\overline{C}^i_{sl} + C^i_w}{C^i_w} = 1 + \frac{\overline{C}^i_{sl}}{C^i_w} \tag{21}$$

with $\overline{C}^i_{sl}$ being the concentration of adsorbed nuclide i in mol per volume of fluid and C^i_w the concentration of dissolved nuclide i in mol per volume of fluid. In the model described here, the concentration of adsorbed nuclide is expressed in mol per mass of surface layer (C^i_{sl}). As the surface layer is considered to be in steady state, the concentration of adsorbed nuclide i is easily calculated once the parameters of the model are constrained (Eq. (4)). Then, the parameter K^i_d can be estimated for each nuclide:

$$K_d^i = \frac{f_s C^i_{sl}}{(1-f_s)C^i_w}. \tag{22}$$

On this basis, the retardation factor can be calculated with the following equation:

$$R_f^i = 1 + \frac{f_s\rho_{sl}(1-\Phi)C^i_{sl}}{(1-f_s)\rho_w\Phi C^i_w}. \tag{23}$$

The calculated concentration in the adsorbed phase takes into account adsorption/desorption but also α-recoil, which implies that the parameter R^i_f is more realistic than if it was based on a simple distribution coefficient. The results of the calculation for each groundwater sample are given in Table 5. K^{Th}_d and K^U_d range from 0.2×10^4 to 5.1×10^4 L kg^{-1} and from 2.5 to 7.9 L kg^{-1}, respectively. K^U_d were independently determined from two experimental studies (Pili et al., 2001). A laboratory batch experiment

Table 5
Retardation coefficients and characteristic time scales for U and Th migration

Sample	K_d^U (L kg^{-1})	K_d^{Th} ($\times 10^4$ L kg^{-1})	R_f^U	R_f^{Th} ($\times 10^4$)	τ_U (yr)	τ_{Th} (Myr)
S1-I	4.9	4.3	20.8	17.4	370	3.09
S1-II	4.9	2.8	20.8	11.4	370	2.03
S2-II	7.9	2.0	33	8.2	587	1.47
G1-II	2.9	1.0	12.7	3.9	226	0.7
G2-II	2.5	5.1	11.1	20.7	197	3.68
G2-II	3.7	2.0	16.0	8.1	284	1.44
G3-III	3	3.9	13.2	15.6	235	2.78
G4-III	5.2	0.2	22.1	1	393	0.17

yielded K_d^U values from 12 to 27 L kg^{-1}. U concentrations measured separately on contaminated chalk cores (1 m long) and the interstitial water extracted by a squeezing technique gave K_d^U ranging from 10 to 30 L kg^{-1}. Therefore, the three determinations of K_d^U are consistent despite the different length scales involved (from cm to km).

Calculated R_f range from 11 to 33 for U and from 1×10^4 to 21×10^4 for Th. Luo et al. (2000) found retardation factors ranging from 0.1×10^3 to 3.4×10^3 for U and from 0.2×10^6 to 18.3×10^6 for Th in a basaltic aquifer. Both U and Th are thus far more mobile in the chalk aquifer. Our R_f values for long-lived thorium (^{230}Th and ^{232}Th) are similar to R_f for ^{234}Th reported by Krishnaswami et al. (1982) for various aquifer materials and ranging from 1.4×10^4 to 2×10^5. Considering the length scale of the studied basin (8 km from the catchment divide to the river) as well as the water velocity in the aquifer (about 450 m yr^{-1}), a characteristic time (τ_i) for nuclide migration from the recharge area to the river, for each element (Table 5), can be estimated with the following equation:

$$\tau_i = \frac{xR_f^i}{v}, \quad (24)$$

where x is the length scale (taken to be 8 km here). For Th migration, the time scale is 400–19,000 times longer than for U. The characteristic time scale ranges from 0.2 to 3.7 Myr for Th and from 200 to 600 yr for U, respectively. These characteristic times could be used for predicting the effect of a contamination in space and time.

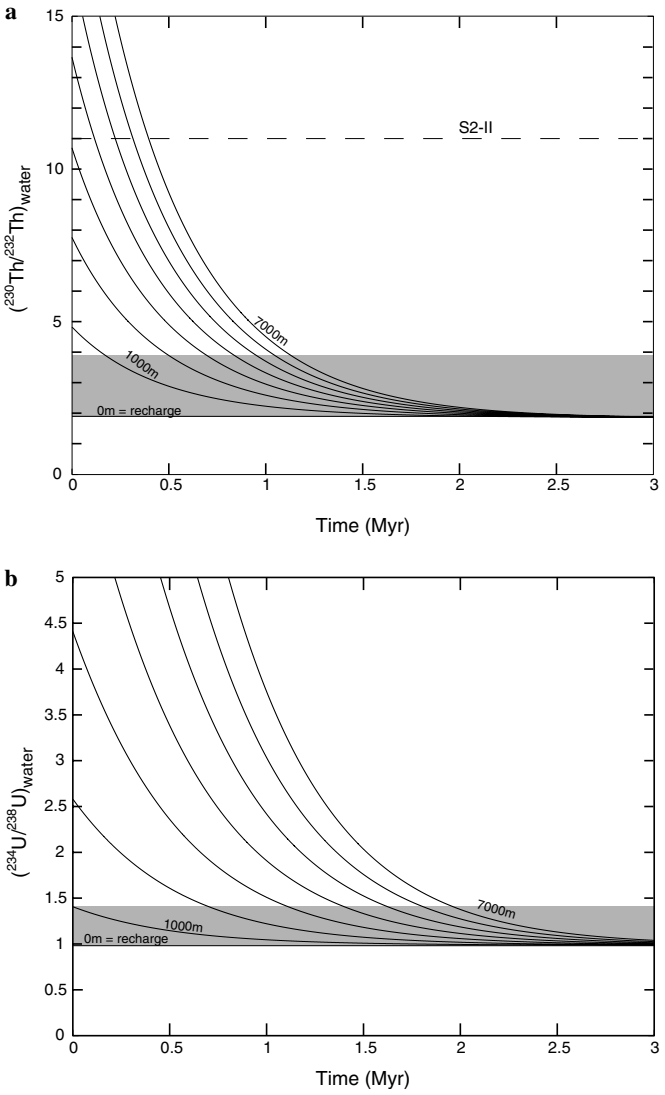

Fig. 10. Model results for the evolution of (a) (^{230}Th/^{232}Th) and (b) (^{234}U/^{238}U) in the groundwater versus time for various distance from the catchment divide. The gray zones represent the range of measured values in the water phase. Both (^{230}Th/^{232}Th) and (^{234}U/^{238}U) increase with distance, but decrease with time. The S2-II sample is shown by a dashed line as it is not on the same flow line. Both systems provide information on the age of the system and indicate that the system in not in steady state.

5.3. Discussion

5.3.1. Assessment of the non-steady-state approach

In our modeling, we have not assumed that the system is at steady state. This modeling approach allows us to follow the time evolution of the nuclide activities in the liquid and solid phases of the aquifer. An unknown parameter still needs to be evaluated in our solution: the age of the system, i.e., the time elapsed since the aquifer became active.

Fig. 10a represents the evolution of (^{230}Th/^{232}Th) in the water as a function of the "age of the system" for different distances from the catchment divide. All the curves show a decrease in (^{230}Th/^{232}Th) with time. At the beginning of the aquifer "operation", the first batch of infiltrating water reacts with a pristine rock that has high quantities of easily leachable ^{234}U and ^{230}Th. This results in a large increase of $(^{230}Th/^{232}Th)_{water}$ within the first meters and years of water circulation. Then, $(^{230}Th/^{232}Th)_{water}$ only decreases with time as shown by modeled curves in Fig. 10a. The solid phase controls the evolution of $(^{230}Th/^{232}Th)_{water}$ until the water/rock system reaches a steady state where activity ratio reaches a constant value regardless of the distance for $t > 2.5$ Myr which is equal to the initial $(^{230}Th/^{232}Th)_{water}$.

The (^{230}Th/^{232}Th) activity ratios measured in the groundwater samples might indicate that the aquifer is younger than 2.5 Myr, because there is a relationship be-

tween the activity ratio and distance (Fig. 7). If the S2-II sample is considered to be an exception, the range in (^{230}Th/^{232}Th) ratios in water indicates that the system is older than 6×10^5 yr.

The same applies for (^{234}U/^{238}U)$_{water}$ (Fig. 10b). After 3 Myr of continuous water circulation, the (^{234}U/^{238}U) ratios reach a steady state controlled by the time scale of U weathering ($W_U = 2 \times 10^{-6}$ yr^{-1}). As shown in Fig. 10b, regardless of the distance, (^{234}U/^{238}U) activity ratios reach asymptotically a common value equal to the initial ($x = 0$) water composition (^{234}U/^{238}U)$_{x=0} = 0.99$ (i.e., the soil leachate). As the data presented in Section 3 show a range in (^{234}U/^{238}U) activity ratios from 1.16 to 1.41 in groundwater, we deduce an age between 0.75 and 1.5 Myr.

The age of the system is thus estimated between 0.6 and 1.5 Myr. This age represents the time when the aquifer became active. As we do not have any other independent determinations, we have estimated an upper limit for the age of the aquifer. The chalk aquifer becomes active with the opening of the fractures, which were due to both decompression of the chalk and freezing–thawing cycles. These processes only take place near the surface, namely in the first hundred meters of rock. Erosion rates in northeastern France have been calculated by Schaller et al. (2001) and range between 14 and 60 mm kyr^{-1} with an average value of 31 mm kyr^{-1}. Given that chalk aquifer is about 100–150 m deep; it will take 3–5 Myr to erode this system. Our estimated age is therefore consistent because it is of the same order of magnitude as the erosion time-scale.

An important result of our modeling is that the system is not at steady state. The main parameter that controls the time to reach steady state is the inverse of the U weathering rate (on the order of 10^6 yr). If we had not analyzed rock samples, we would have assumed that the system is at steady state as in previous studies, but our results show that it is not the case.

Our model is also able to predict the time evolution of a U contamination in the system. A transient solution is needed to describe the propagation of the perturbation in the aquifer. As U is less surface-reactive than Th, a perturbation in the system will not be damped by the interaction with the solid. The characteristic time scale of migration and the time scale for reaching steady state are not similar. The evolution of the natural system is governed by the weathering of the solid, while in the case of contamination, the perturbation in the system is brought by the water and the relevant time scales are estimated in Section 5.2.3.

5.3.2. Consistency of the model with the observations

The complexity of transport processes in a heterogeneous media prevents our model from explaining all the observed data. In this section, we discuss where our 1-D single porosity model fails to account for some important observations, and potential reasons for these discrepancies. This could help identify where more sophisticated modeling could be used to fully account for our observations.

First, as the chalk is heterogeneous, it is highly likely that permeabilities are locally variable, at the scale of hundreds of meters (for example in the dry valleys). This might explain why the trend of (^{230}Th/^{232}Th) versus distance cannot be explained by a single value for the flow velocity. The required range of water velocities (Fig. 7) is well within the variability of permeability obtained from a complete hydrological modeling of the chalk aquifer (F. Renard, pers. comm.) as well as for other areas of the same aquifer (Price et al., 1993).

The weathering rates of U and Th have been assumed to be different because these elements are located in different phases (carbonates versus silicates, respectively). In this case, ^{230}Th and ^{232}Th must behave differently because ^{230}Th is contained in the carbonate phase whereas ^{232}Th is located mainly in the non-carbonate phase. As carbonates dissolve faster than silicate rocks, one must have $W_{^{230}Th} > W_{^{232}Th}$. With this hypothesis, the (^{230}Th/^{232}Th) in groundwater would increase over a shorter distance than previously shown in Fig. 7: for $W_{^{230}Th} = W_U$, the predicted (^{230}Th/^{232}Th) in groundwater are higher than the observed ratios by up to a factor of 5.

There is an additional for the preferential release of ^{230}Th relative to ^{232}Th. As discussed in Section 5.2.2, the recoil of ^{230}Th enhances its mobilization in the solution (parameter $\varepsilon_{^{230}Th}$). Because of this added complexity in the case of Th, it is difficult to deconvolve the respective role of incongruent dissolution and recoil effects.

Our model does not include a complete description of the major element chemistry of the waters. In order to explain the (^{234}U/^{238}U) > 1, the U-series model would need to be coupled with a model for the water chemistry. This approach would require repeated sampling of water throughout a hydrological cycle and is beyond the scope of this study.

Similar (^{230}Th/^{232}Th) in the water and surface layer are not readily explained by a model where the length scale for Th adsorption is approximately a few meters. The interpretation we propose is that the fractures in the chalk represent a hydrological by-pass that permits the rapid transport of 'dissolved' Th to deeper layers in the aquifer. In this case, the length scale of Th transport in the aquifer is substantially greater. Obviously, a more complete model would include a double-porosity description of the aquifer.

Admittedly, a 1-D continuum model cannot provide a full interpretation. Yet, this modeling is a clear step forward in the identification of key processes controlling the migration of U-series nuclides in high transmittivity aquifers. The relative role of transport through matrix or fractures will be addressed in future studies.

6. Conclusions

Uranium and thorium isotopes were measured in rock and water samples of an unconfined chalk aquifer in order to constrain processes affecting radionuclide transport. We have developed precise measurements of (^{230}Th/^{232}Th) in low level samples by MC-ICPMS to characterize Th isotopic composition in this aquifer. This study shows the mobility of U within the aquifer, with preferential leaching of ^{234}U in the upper part of the aquifer and reprecipitation in the zone of water-table fluctuation. Thorium is less affected by weathering because it is hosted by minor phases in the chalk that are more resistant to dissolution, and is mostly transported in the aquifer by colloids derived from the recharge zone. A systematic enrichment of ^{230}Th over ^{238}U has been observed, due to preferential weathering of U in the rock. Hence, (^{230}Th/^{238}U) ratios greater than 1 are principally due to U leaching. Th adsorption plays a minor role due to the small volume of the surface layer relative to the grain size. Our results exemplify the importance of understanding the water recharge process within the aquifer and the role of fractures in the infiltration of rainwater to the water table on water chemistry.

We have developed a 1-D model in order to constrain the parameters controlling the U-series disequilibria measured in the different phases of the aquifer. Uranium weathering rate, U and Th distribution coefficients and recoil effects have been evaluated. The rock dissolution is incongruent due to the presence of non-carbonate phases ($W_U \neq W_{Th}$). We have derived from these parameters the characteristic time scale of U and Th migration within this aquifer. The results of the modeling show that U is more mobile in chalk aquifers than in other groundwater systems, such as sandy or basaltic aquifers, described by earlier studies. Estimated retardation factors are <33 for U and between 1×10^4 and 21×10^4 for Th. As this model describes a transient behavior of the radionuclides, it can be used for estimating rates of anthropogenic nuclide migration.

Acknowledgments

We thank Bruno Lanson (LGIT Grenoble) for XRD analysis, Caroline Gorge at IPGP for major elements and Sr isotopic analysis in water samples, Pascale Louvat for her help in ICP-MS measurements and Monique Pierre for her help with chemical separations. At CEA, Pierre Crançon, Walter Epting, Patricia Gilbert, François Renard and Patrick Richon are thanked for their help during different stages of this work. The authors greatly acknowledge Ben Reyolds for his constructive comments which helped improve the manuscript, Don Porcelli and three anonymous reviewers for their constructive reviews, and S. Krishnaswami for his editorial handling and editing of the manuscript.

Associate editor: S. Krishnaswami

Appendix A. Sampling and analytical procedures

A.1. Chemical separations

Aliquots of 200 ml acidified water samples were spiked with ^{236}U and ^{229}Th. U and Th contents were measured by isotopic dilution after separating them by anion-exchange chromatography (Manhès, 1981).

For rock analysis, about 200 mg samples were powdered and first digested in acetic acid to dissolve carbonates. The slurry was centrifuged, and the supernatant was extracted and dried on a hot plate. The residue was then dissolved in concentrated HF–HNO_3. U/Th were separated from solutions and purified using anion-exchange resins. Material coating fracture wall within the carbonates was also collected by scraping with a spatula. U/Th isotopes were measured in these samples (200 mg) following the procedure described above for the chalk samples.

Total procedural blanks for rock and water samples were 25 pg for ^{238}U, for ^{232}Th it was 14 pg for water and 35 pg for rock samples. (^{234}U/^{238}U) and (^{230}Th/^{232}Th) ratios and U and Th concentrations in rocks and waters were determined by thermal ionization mass spectrometry (TIMS). Th and U isotopic ratios in waters were determined using multi-collector inductively coupled plasma mass spectrometry (MC-ICP-MS) (see Table A.1).

Strontium isotope composition of water samples was determined using the procedure developed by Meynadier et al. (2006). Strontium separation was performed automatically using high-performance ion chromatography (HPIC). Samples were loaded on degassed single W filaments. ^{87}Sr/^{86}Sr isotope ratios were measured on a VG-354 mass spectrometer. Measurements of the SRM-987 Sr standard yielded $^{87}Sr/^{86}Sr = 0.710271 \pm 8$ ($n = 20$, $2\sigma_m$) (certified value 0.710235 ± 0.000017). For rock samples, strontium isotope ratios' measurements were done by Actlabs (Canada). Samples were dissolved in a mixture of HF, HNO_3 and $HClO_4$. Prior to dissolution, all samples were spiked with a ^{85}Rb–^{84}Sr mixed solution. Rb and Sr were separated using conventional cation-exchange techniques. The analyses were done on a Finnigan MAT 261 mass spectrometer equipped with 8-collector, in a static mode. Over the period of measurements, the weighted average of 15 SRM-987 Sr-standard runs yielded $^{87}Sr/^{86}Sr = 0.710261 \pm 12$ (2σ).

A.2. Thermal ionization mass spectrometry (TIMS) procedure for U/Th analyses in rock samples

Measurements were performed on a Thermo-Finnigan Triton mass spectrometer. Uranium samples were loaded on a degassed single Re filament between two colloidal graphite layers and dried at a temperature of 1720 °C. Thorium samples were loaded on degassed double Re filament between two layers of H_3PO_4. The concentration measurements have an uncertainty less than 0.35% for U and less than 1% for Th at the 2σ level (σ is the standard deviation). Reproducibility for ^{234}U/^{238}U ratios was determined using NBS-960 standard (now CRM-145, also called NBL-112a) on 16 aliquots and was 0.4% at the 2σ level with a mean value of $5.287\ (\pm 0.02) \times 10^{-5}$. Repeated analysis of ThS1 standard gave a reproducibility of 1% on (^{230}Th/^{232}Th) activity ratio with a mean value of 1.023 ± 4 ($n = 7$; 2σ) which is in good agreement with the value of 1.020 ± 0.002 obtained by Claude-Ivanaj et al. (1998).

Table A.1
Cup configurations for uranium and thorium acquisition on a MC-ICP-MS

Cup #	L1	SEM	H1	H2	H3
Uranium		^{234}U	^{235}U	^{236}U	^{238}U
Thorium	^{229}Th	^{230}Th		^{232}Th	
		229.7			
		230.4			

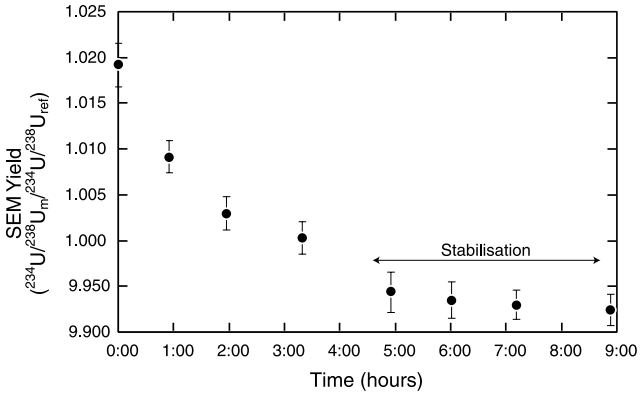

Fig. A.1. Variation of the secondary electron multiplier (SEM) yield over 9 h of continuous operation of the plasma. Yield = $(^{234}U/^{238}U)_{measured}/(^{234}U/^{238}U)_{ref}$.

A.3. Inductively coupled plasma mass spectrometry (ICP-MS) procedure for U/Th analyses in water samples

Due to a very low Th concentration (<100 pg L^{-1}) in natural water, analyses were not possible by TIMS, so MC-ICP-MS was utilized for the precise determination of $^{230}Th/^{232}Th$ isotopic ratios in water samples (Luo et al., 1997; Turner et al., 2001). Measurements were performed on a Thermo-Finnigan Neptune equipped with a double spray chamber. Both samples and standard solutions were diluted in 2% HNO_3. We first tuned the instrument for U measurements to follow the evolution of mass bias as well as the yield of the ion counting channel (relative to Faraday cups) using a 12 ppb U solution of NBS-960 standard. The ionization efficiency for U and Th was 0.25% and 0.12%, respectively. During measurements, the intensity of the signal remained relatively constant within 1%.

A.3.1. Ion counting yield calibration

NBS-960 standard was used before and after each sample in order to determine a yield calibration for the ion counting channel relative to Faraday cups. Th measurements were performed once the plasma was stable and yielded constant U isotopic ratios with standard solutions. It was noticed that the yield was stable after 4 h of continuous operation (Fig. A.1).

A.3.2. Correction for ^{232}Th tail contribution

The tail of ^{232}Th on ^{230}Th can contribute 3–6% of the ^{230}Th signal. We determined for each sample and standard the tail contribution of the ^{232}Th peak on the ^{230}Th peak. The tail correction was estimated using only two masses (230.4 and 229.7) and fitted with an exponential law. This yields the same results as with four masses but is less time consuming.

A.3.3. Mass bias

Th mass fractionation was corrected using $(^{230}Th/^{232}Th)$ data of a standard (Th_105, given by C. Innocent (BRGM, Orléans)) before and after each sample, and by applying an exponential mass-dependent fractionation law.

A.3.4. Reproducibility

The reproducibility of $(^{234}U/^{238}U)$ activity ratios was determined by analyzing three different aliquots of the same sample G2 and was found to be 0.4% at the 2σ level. Th isotope measurements of water samples could only be done once, because of the small sample size (0.6–12 ng). We determined the reproducibility of $(^{230}Th/^{232}Th)$ activity ratio using standard Th S1 on 11 aliquots with a concentration of 10 ppb in ^{232}Th (with a consumption of 1.2 ml of solution per analysis), and obtained 0.75% at the 2σ level with a mean value of 1.017 ± 0.008.

References

Andrews, J.N., Kay, R.L.F., 1982. $^{234}U/^{238}U$ activity ratios of dissolved uranium in groundwaters from a Jurassic Limestone in England. *Earth Planet. Sci. Lett.* **57**, 139–151.

Bonotto, D.M., Andrews, J.N., 1993. The mechanism of $^{234}U/^{238}U$ activity ratio enhancement in karestic limestone groundwater. *Chem. Geol.* **103**, 193–206.

Bourdon, B., Turner, S., Henderson, G.M., Lundstrom, C.C., 2003. Introduction to U-series geochemistry. In: Bourdon, B., Henderson, G.M., Lundstrom, C.C., Turner, S.P. (Eds.), *Uranium-Series Geochemistry*, vol. 52. Min. Soc. America, Washington, DC, pp. 1–21.

Buddemeier, R.W., 1988. Transport of colloidal contaminants in groundwater: radionuclide migration at Nevada Test Site. *Appl. Geochem.* **3**, 535–548.

Cacheris, W.P., Choppin, G.R., 1987. Dissociation kinetics of thorium–humate complex. *Radiochim. Acta* **42**, 185–190.

Claude-Ivanaj, C., Bourdon, B., Allègre, C.J., 1998. Ra–Th–Sr isotope systematics in Grande Comore Island: a case study of plume–lithosphere interaction. *Earth Planet. Sci. Lett.* **164**, 99–117.

Copenhaver, S.A., Krishnaswami, S., Turekian, K.K., Epler, N., Cochran, J.K., 1993. Retardation of ^{238}U and ^{232}Th decay chain radionuclides in Long Island and Connecticut aquifers. *Geochim. Cosmochim. Acta* **57**, 597–603.

Crampon, N., Roux, J.C., Bracq, P., 1993a. Hydrogeology of the chalk in France. *Hydrogéologie* **2**, 81–123.

Crampon, N., Roux, J.C., Bracq, P., Delay, F., Lepiller, M., Mary, G., Rasplus, L., Alcaydé, G., 1993b. France. In: Downing, R.A., Price, M., Jones, G.P. (Eds.), *The Hydrogeology of the Chalk of North West Europe*. Oxford Science Publications, Oxford, pp. 113–152.

Cuttell, J.C., Lloyd, J.W., Ivanovich, M., 1986. A study of uranium and thorium series isotopes in chalk groundwaters of Lincolnshire, U.K. *J. Hydrol.* **86**, 343–365.

Dosseto, A., Bourdon, B., Gaillardet, J., Allègre, C.J., Filizola, N., 2006. Time scale and conditions of weathering under tropical climate: study of the Amazon basin with U-series. *Geochim. Cosmochim. Acta* **70**, 71–89.

Doyle, C.S., Kendelewicz, T., Brown Jr., G.E., 2004. Inhibition of the reduction of Cr(VI) at the magnetite–water interface by calcium carbonate coatings. *Appl. Surf. Sci.* **230**, 260–271.

Edmunds, W.M., Cook, J.M., Darling, W.G., Kinniburgh, D.G., Miles, D.L., Bath, A.H., Morgan-Jones, M., Andrews, J.N., 1987. Baseline geochemical conditions in the Chalk aquifer, Berkshire, U.K.: a basis for groundwater quality management. *Appl. Geochem.* **2**, 251–274.

Elliot, T., Andrews, J.N., Edmunds, W.M., 1999. Hydrochemical trends, palaeorecharge and groundwater ages in the fissured Chalk aquifer of the London and Berkshire Basins, UK. *Appl. Geochem.* **14**, 333–363.

Feast, N.A., Hiscock, K.M., Dennis, P.F., Bottrell, S.H., 1997. Controls on stable isotope profiles in the Chalk aquifer of north-east Norfolk, UK, with special reference to dissolved sulphate. *Appl. Geochem.* **12**, 803–817.

Henderson, G.M., Slowey, N.C., 2000. Evidence from U–Th dating against Northern Hemisphere forcing of the penultimate deglaciation. *Nature* **404**, 61–66.

Hubert, A., 2005. Géochimie des séries de l'uranium dans les aquifères: cas de l'aquifère de la craie (Champagne, France). Ph.D. thesis. IPG Paris, 242pp.

Ivanovich, M., Harmon, R.S., 1992. *Uranium-Series Disequilibrium: Applications to Earth, Marine, and Environmental Sciences*. Oxford University Press, Oxford.

Kersting, A.B., Efurd, D.W., Finnegan, D.L., Rokop, D.J., Smith, D.K., Thompson, J.L., 1999. Migration of plutonium in ground water at the Nevada Test Site. *Nature* **397**, 56–59.

Keum, D.K., Hahn, P.S., 2003. A coupled reactive chemical transport model: mixing cell model with two solid phases and its application. *Comput. Geosci.* **29**, 431–445.

Kigoshi, K., 1971. Alpha recoil thorium-234: dissolution into water and uranium-234/uranium-238 disequilibrium in nature. *Science* **173**, 47–49.

Kloppmann, W., Dever, L., Edmunds, W.M., 1996. Redox zones in the Chalk aquifer of the Paris and North German basins. *Hydrol. Sci.* **41** (3), 311–326.

Kloppmann, W., Dever, L., Edmunds, W.M., 1998. Residence time of Chalk groundwaters in the Paris Basin and the North German Basin: a geochemical approach. *Appl. Geochem.* **13** (5), 593–606.

Krishnaswami, S., Graustein, W.C., Turekian, K.K., Dowd, J.F., 1982. Radium, thorium and radioactive lead isotopes in groundwaters: application to in situ determination of adsorption-desorption rate constants and retardation factors. *Water Resour. Res.* **18** (6), 1663–1675.

Ku, T.-L., Luo, S., Leslie, B.W., Hammond, D.E., 1992. Decay-series disequilibria applied to the study of rock–water interaction and geothermal system. In: Ivanovich, M., Harmon, R.S. (Eds.), *Uranium-Series Disequilibrium: Applications to Earth, Marine, and Environmental Sciences*. Oxford University Press, Oxford, pp. 631–668.

Langmuir, D., Herman, J.S., 1980. The mobility of thorium in natural waters at low temperatures. *Geochim. Cosmochim. Acta* **44**, 1753–1766.

Little, R., Muller, E., Mackay, R., 1996. Modelling of contaminant migration in a chalk aquifer. *J. Hydrol.* **175**, 473–509.

Liu, J., Yu, J.-W., Neretnieks, I., 1996. Transport modelling in the natural analogue study of the Cigar Lake uranium deposit (Saskatchewan, Canada). *J. Contam. Hydrol.* **21**, 19–34.

Luo, S., Ku, T.-L., Roback, R., Murrell, M., McLing, T.L., 2000. In-situ radionuclide transport and preferential groundwater flows at INEEL (Idaho): decay-series disequilibrium studies. *Geochim. Cosmochim. Acta* **64** (5), 867–881.

Luo, X., Rehkämper, M., Lee, D.-C., Halliday, A.N., 1997. High precision $^{230}Th/^{232}Th$ and $^{234}U/^{238}U$ measurements using energy-filtered ICP magnetic sector multiple collector mass spectrometry. *Int. J. Mass Spectrom. Ion Process.* **171**, 105–117.

Maher, K., DePaolo, D.J., Lin, J.Chiu-Fang, 2004. Rates of silicate dissolution in deep-sea sediment: in situ measurement using $^{234}U/^{238}U$ of pore fluids. *Geochim. Cosmochim. Acta* 68 (22), 4629–4648.

Manhès, G., 1981. Développement de l'ensemble chronométrique U–Th–Pb : contribution à la chronologie initiale du système solaire. Thèse d'état, Université Paris 6.

Meynadier, L., Gorge, C., Birck, J.-L., Allègre, C.J., 2006. Automatic separation for isotopic analysis: a fast, automatic strontium element separation by HPIC. *Chem. Geol.* **227** (1-2), 26–36.

Osmond, J.K., Cowart, J.B., 1992. Ground water. In: Ivanovich, M., Harmon, R.S. (Eds.), *Uranium-Series Disequilibrium: Applications to Earth, Marine, and Environmental Sciences*. Oxford University Press, Oxford, pp. 290–333.

Osmond, J.K., Ivanovich, M., 1992. Uranium-series mobilization and surface hydrology. In: Ivanovich, M., Harmon, R.S. (Eds.), *Uranium-Series Disequilibrium: Applications to Earth, Marine, and Environmental Sciences*. Oxford University Press, Oxford, pp. 259–289.

Pili, E., Guinois, G., Crançon, P., 2001. Uranium migration in chalk from top to bottom. *ECORAD Conference abstracts* **P1M/18** (171).

Plater, A.J., Ivanovich, M., Dugdale, R.E., 1992. uranium series disequilibrium in river sediments and waters: the significance of anomalous activity ratios. *Appl. Geochem.* **7**, 101–110.

Porcelli, D., Andersson, P.S., Baskaran, M., Wasserburg, G.J., 2001. Transport of U- and Th-series nuclides in a Baltic Shield watershed and the Baltic Sea. *Geochim. Cosmochim. Acta* **65** (15), 2439–2459.

Porcelli, D., Andersson, P.S., Wasserburg, G.J., Ingri, J., Baskaran, M., 1997. The importance of colloids and mires for the transport of uranium isotopes through the Kalix River watershed and Baltic Sea. *Geochim. Cosmochim. Acta* **61** (19), 4095–4113.

Porcelli, D., Swarzenski, P.W., 2003. The behavior of U- and Th-series nuclides in groundwater. In: Bourdon, B., Henderson, G.M., Lundstrom, C.C., Turner, S.P. (Eds.), *Uranium-Series Geochemistry*, vol. 52. Min. Soc. America, Washington, DC, pp. 317–361.

Price, M., Downing, R.A., Edmunds, W.M., 1993. The chalk as an aquifer. In: Downing, R.A., Price, M., Jones, G.P. (Eds.), *The Hydrogeology of the Chalk of North West Europe*. Oxford Science Publications, Oxford, pp. 35–58.

Reynolds, B.C., Wasserburg, G.J., Baskaran, M., 2003. The transport of U- and Th-series nuclides in sandy confined aquifers. *Geochim. Cosmochim. Acta* **67** (11), 1955–1972.

Riotte, J., Chabaux, F., 1999. ($^{234}U/^{238}U$) Activity ratios in freshwaters as tracers of hydrological processes: the Strengbach watershed (Vosges, France). *Geochim. Cosmochim. Acta* **63** (9), 1263–1275.

Schaller, M., von Blanckenburg, F., Hovius, N., Kubik, P.W., 2001. Large-scale erosion rates from in situ-produced cosmogenic nuclides in European river sediments. *Earth Planet. Sci. Lett.* **188**, 441–458.

Schürch, M., Edmunds, W.M., Buckley, D., 2004. Three-dimensional flow and trace metal mobility in shallow Chalk groundwater, Dorset, United Kingdom. *J. Hydrol.* **292** (1-4), 229–248.

Tricca, A., Porcelli, D., Wasserburg, G.J., 2000. Factors controlling the groundwater transport of U, Th, Ra and Rn. *Proc. Indian Acad. Sci.—Earth Planet. Sci.* **109** (1), 95–108.

Tricca, A., Wasserburg, G.J., Porcelli, D., Baskaran, M., 2001. The transport of U- and Th-series nuclides in a sandy unconfined aquifer. *Geochim. Cosmochim. Acta* **65** (8), 1187–1210.

Turner, S., Van Calsteren, P., Vigier, N., Thomas, L., 2001. Determination of thorium and uranium isotope ratios in low-concentration geological materials using a fixed multi-collector-ICP-MS. *J. Anal. Atom. Spectrom.* **16**, 612–615.

Vachier, P., Cambier, P., Prost, R., 1979. Structure d'un milieu poreux : la craie. *Ann. Agron.* **30** (3), 247–263.

Vachier, P., Dever, L., Fontes, J.-C., 1987. Mouvements de l'eau dans la zone non saturée et alimentation de la nappe de la craie de champagne (France). In: *Isotope Techniques in Water Resources Development, Vienna, IAEA Conference*, pp. 367–379.

van der Lee, J., De Windt, L., 2002. *CHESS Tutorial and Cookbook*. Ecole des Mines de Paris, CIG Fontainebleau, 112pp.

Viers, J., Dupré, B., Polvé, M., Schott, J., Dandurand, J.-L., Braun, J.-J., 1997. Chemical weathering in the drainage basin of a tropical watershed (Nsimi-Zoetele site, Cameroon): comparison between organic-poor and organic-rich waters. *Chem. Geol.* **140**, 181–206.

Vigier, N., Bourdon, B., Turner, S., Allègre, C.J., 2001. Erosion timescales derived from U-decay series measurements in rivers. *Earth Planet. Sci. Lett.* **193**, 549–563.

Vigier, N., Bourdon, B., Turner, S., Van Calsteren, P., Subramanian, V., Dupré, B., Allègre, C.J., 2005. Parameters influencing the duration and rates of weathering deduced from U-series measured in rivers: the Deccan Trap region (India). *Chem. Geol.* **219**, 69–91.

Zielinski, R.A., Rosholt, J.N., 1978. Uranium in waters ans aquifer rocks at the Nevada Test Site, Nye County, Nevada. *J. Res. US Geol. Surv.* **6** (4), 489–498.